Fast Finite Shearlet Transform: a tutorial

Sören Häuser*

February 9, 2012

arXiv:1202.1773v1 [math.NA] 8 Feb 2012

Contents

1 Introduction

In recent years, much effort has been spent to design directional representation systems for images such as curvelets [1], ridgelets [2] and shearlets [10] and corresponding transforms (this list is not complete). Among these transforms, the shearlet transform stands out since it stems from a square-integrable group representation [4] and has the corresponding useful

*University of Kaiserslautern, Dept. of Mathematics, Kaiserslautern, Germany, haeuser@mathematik.uni-kl.de

mathematical properties. Moreover, similarly as wavelets are related to Besov spaces via atomic decompositions, shearlets correspond to certain function spaces, the so-called shearlet coorbit spaces [5]. In addition shearlets provide an optimally sparse approximation in the class of piecewise smooth functions with C^2 singularity curves, i.e.,

$$\|f - f_N\|_{L_2}^2 \leq CN^{-2}(\log N)^3 \quad \text{as } N \to \infty,$$

where f_N is the nonlinear shearlet approximation of a function f from this class obtained by taking the N largest shearlet coefficients in absolute value.

Shearlets have been applied to a wide field of image processing tasks, see, e.g., [7, 11, 12, 17]. In [9] the authors showed how the directional information encoded by the shearlet transform can be used in image segmentation. Fig 1 illustrates the directional information in the shearlet coefficients. To this end, we introduced a simple discrete shearlet transform which translates the shearlets over the full grid at each scale and for each direction. Using the FFT this transform can be still realized in a fast way. This tutorial explains the details behind the MATLAB-implementation of the transform and shows how to apply the transform. The software is available for free under the GPL-license at

`http://www.mathematik.uni-kl.de/~haeuser/FFST/`

In analogy with other transforms we named the software *FFST* – **F**ast **F**inite **S**hearlet **T**ransform. The package provides a fast implementation of the finite (discrete) shearlet transform.

(a) Forms with different edge orientations

(b) Shearlet coefficients for $a = \frac{1}{64}$ and $s = -1$

(c) Sum of shearlet coefficients for $a = \frac{1}{64}$ for all s

Figure 1: Shearlet coefficients can detect edges with different orientations.

This tutorial is organized as follows: In Section 2 we introduce the continuous shearlet transform and prove the properties of the involved shearlets. We follow in Section 3 the path via the continuous shearlet transform, its counterpart on cones and finally its discretization on the full grid to obtain the translation invariant discrete shearlet transform. This is different to other implementations as, e.g., in *ShearLab*[1], see [16]. Our discrete shearlet transform can be efficiently computed by the fast Fourier transform (FFT). The discrete shearlets constitute a Parseval frame of the finite Euclidean space such that the inversion of the shearlet transform

[1] http://www.shearlab.org

can be simply done by applying the adjoint transform. The second part of the section covers the implementation and installation details and provides some performance measures.

2 Shearlet transform

In this section we combine some mostly well-known results from different authors. To make this paper self-contained and to obtain a complete documentation we also include the proofs. The functions where taken from [15, 14]. The construction of the shearlets is based on ideas from [12] and [13]. The shearlet transform and the concept of shearlets n the cone was introduced in [6].

2.1 Some functions and their properties

To define usable shearlets we need functions with special properties. We begin with defining these functions and prove their necessary properties. The results will be used later. The following results are taken basically from [12] and [13].

We start by defining an auxiliary function $v\colon \mathbb{R} \to \mathbb{R}$ as

$$v(x) := \begin{cases} 0 & \text{for } x < 0 \\ 35x^4 - 84x^5 + 70x^6 - 20x^7 & \text{for } 0 \le x \le 1 \\ 1 & \text{for } x > 1. \end{cases} \tag{1}$$

This function was proposed by Y. Meyer in [15, 14]. Other choices of v are possible, in [16] the simpler function

$$\widetilde{v}(x) = \begin{cases} 0 & \text{for } x < 0 \\ 2x^2 & \text{for } 0 \le x \le \frac{1}{2} \\ 1 - 2(1-x)^2 & \text{for } \frac{1}{2} \le x \le 1 \\ 1 & \text{for } x > 1 \end{cases}$$

was chosen. As we will see the useful properties of v for our purposes are its symmetry around $(\frac{1}{2}, \frac{1}{2})$ and the values at 0 and 1 with increase in between. A plot of v is shown in Fig. 2(a).

Next we define the function $b : \mathbb{R} \to \mathbb{R}$ with

$$b(\omega) := \begin{cases} \sin(\frac{\pi}{2} v(|\omega| - 1)) & \text{for } 1 \le |\omega| \le 2 \\ \cos(\frac{\pi}{2} v(\frac{1}{2}|\omega| - 1)) & \text{for } 2 < |\omega| \le 4 \\ 0 & \text{otherwise,} \end{cases} \tag{2}$$

where b is symmetric, positive, real and $\operatorname{supp} b = [-4, -1] \cup [1, 4]$. We further have that $b(\pm 2) = 1$. A plot of b is shown in Fig. 2(b).

Because of the symmetry we restrict ourselves in the following analysis to the case $\omega > 0$. Let $b_j := b(2^{-j}\cdot)$, $j \in \mathbb{N}_0$, thus, $\operatorname{supp} b_j = 2^j[1, 4] = [2^j, 2^{j+2}]$ and $b_j(2^{j+1}) = 1$. Observe that b_j is increasing for $\omega \in [2^j, 2^{j+1}]$ and decreasing for $\omega \in [2^{j+1}, 2^{j+2}]$. Obviously all these properties

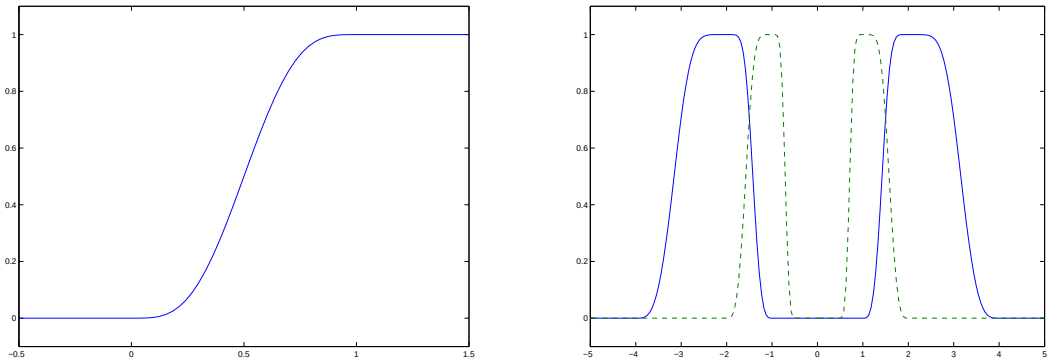

(a) $v(x)$ (b) solid: $b(\omega)$, dashed: $b(2\omega)$

Figure 2: The two auxiliary functions v in (1) and b in (2)

carry over to b_j^2. These facts are illustrated in the following diagram where $\nearrow$ stands for the increasing function and $\searrow$ for decreasing function.

$$\begin{array}{c|ccccccc} \omega & 2^j & & 2^{j+1} & & 2^{j+2} & & 2^{j+3} \\ b_j & 0 & \nearrow & 1 & \searrow & 0 & & \\ b_{j+1} & & & 0 & \nearrow & 1 & \searrow & 0 \end{array}$$

For $j_1 \neq j_2$ the overlap between the support of $b_{j_1}^2$ and $b_{j_2}^2$ is empty except for $|j_1 - j_2| = 1$. Thus, for b_j^2 and b_{j+1}^2 we have that $\operatorname{supp} b_j^2 \cap \operatorname{supp} b_{j+1}^2 = [2^{j+1}, 2^{j+2}]$. In this interval b_j^2 is decreasing with $b_j^2 = \cos^2(\frac{\pi}{2} v(\frac{2^{-j}}{2}|\omega| - 1))$ and b_{j+1}^2 is increasing with $b_{j+1}^2 = \sin^2(\frac{\pi}{2} v(2^{-(j+1)}|\omega| - 1))$. We get for their sum in this interval

$$b_j^2(\omega) + b_{j+1}^2(\omega) = \cos^2\left(\frac{\pi}{2} v(2^{-j-1}|\omega| - 1)\right) + \sin^2\left(\frac{\pi}{2} v(2^{-j-1}|\omega| - 1)\right) = 1.$$

Hence, we can summarize

$$(b_j^2 + b_{j+1}^2)(\omega) = \begin{cases} b_j^2 & \text{for } \omega < 2^{j+1} \\ 1 & \text{for } 2^{j+1} \leq \omega \leq 2^{j+2} \\ b_{j+1}^2 & \text{for } \omega > 2^{j+2}. \end{cases}$$

Consequently, we have the following lemma

Lemma 2.1. *For b_j defined as above, the relations*

$$\sum_{j=-1}^{\infty} b_j^2(\omega) = \sum_{j=-1}^{\infty} b^2(2^{-j}\omega) = 1 \quad \textit{for } |\omega| \geq 1$$

and

$$\sum_{j=-1}^{\infty} b_j^2(\omega) = \begin{cases} 0 & \textit{for } |\omega| \leq \frac{1}{2} \\ \sin^2\left(\frac{\pi}{2} v(2\omega - 1)\right) & \textit{for } \frac{1}{2} < |\omega| < 1 \\ 1 & \textit{for } |\omega| \geq 1 \end{cases} \tag{3}$$

hold true.

Proof. In each interval $[2^{j+1}, 2^{j+2}]$ only b_j and b_{j+1}, $j \geq -1$, are not equal to zero. Thus, it is sufficient to prove that $b_j^2 + b_{j+1}^2 \equiv 1$ in this interval. We get that

$$\begin{aligned}(b_j^2 + b_{j+1}^2)(\omega) = \; & b^2(\underbrace{2^{-j}\omega}_{\in\, 2^{-j}[2^{j+1},\, 2^{j+2}] \,=\, [2,\,4]}) \quad + \quad b^2(\underbrace{2^{-j-1}\omega}_{\in\, 2^{-j-1}[2^{j+1},\, 2^{j+2}] \,=\, [1,\,2]}) \\ &= \cos^2\left(\frac{\pi}{2} v(\frac{1}{2}\cdot 2^{-j}\omega - 1)\right) + \sin^2\left(\frac{\pi}{2} v(2^{-j-1}\omega - 1)\right) \\ &= \cos^2\left(\frac{\pi}{2} v(2^{-j-1}\omega - 1)\right) + \sin^2\left(\frac{\pi}{2} v(2^{-j-1}\omega - 1)\right) \\ &= 1.\end{aligned}$$

The second relation follows by straightforward computation. □

Recall that the *Fourier transform* $\mathcal{F}\colon L_2(\mathbb{R}^2) \to L_2(\mathbb{R}^2)$ and the inverse transform are defined by

$$\begin{aligned}\mathcal{F}f(\omega) = \hat{f}(\omega) &:= \int_{\mathbb{R}^2} f(t) e^{-2\pi i \langle \omega, t\rangle} dt, \\ \mathcal{F}^{-1}\hat{f}(\omega) = f(t) \; &= \int_{\mathbb{R}^2} \hat{f}(\omega) e^{2\pi i \langle \omega, t\rangle} d\omega.\end{aligned}$$

Now we define the function $\psi_1\colon \mathbb{R} \to \mathbb{R}$ via its Fourier transform as

$$\hat{\psi}_1(\omega) := \sqrt{b^2(2\omega) + b^2(\omega)}. \tag{4}$$

Fig. 3(a) shows the function. The following theorem states an important property of ψ_1.

Theorem 2.2. *The above defined function $\hat{\psi}_1$ has $\operatorname{supp}\hat{\psi}_1 = [-4, -\frac{1}{2}] \cup [\frac{1}{2}, 4]$ and fulfills*

$$\sum_{j\geq 0} |\hat{\psi}_1(2^{-2j}\omega)|^2 = 1 \quad \textit{for } |\omega| > 1.$$

Proof. The assumption on the support follows from the definition of b. For the sum we have

$$\begin{aligned}\sum_{j\geq 0} |\hat{\psi}_1(2^{-2j}\omega)|^2 &= \sum_{j=0}^{\infty} b^2(2\cdot 2^{-2j}\omega) + b^2(2^{-2j}\omega) \\ &= \sum_{j=0}^{\infty} b^2(2^{-2j+1}\omega) + b^2(2^{-2j}\omega),\end{aligned}$$

where $-2j+1 \in \{+1, -1, -3, \ldots\}$ (odd) and $-2j \in \{0, -2, -4, \ldots\}$ (even). Thus, by Lemma 2.1, we get

$$\begin{aligned}\sum_{j\geq 0} |\hat{\psi}_1(2^{-2j}\omega)|^2 &= \sum_{j=-1}^{\infty} b^2(2^{-j}\omega) \\ &= 1.\end{aligned}$$

□

By (3) we have that

$$\sum_{j\geq 0} |\hat{\psi}_1(2^{-2j}\omega)|^2 = \begin{cases} 0 & \text{for } |\omega| \leq \frac{1}{2} \\ \sin^2\left(\frac{\pi}{2} v(2\omega - 1)\right) & \text{for } \frac{1}{2} < |\omega| < 1 \\ 1 & \text{for } |\omega| \geq 1. \end{cases} \tag{5}$$

Next we define a second function $\psi_2 \colon \mathbb{R} \to \mathbb{R}$ – again in the Fourier domain – by

$$\hat{\psi}_2(\omega) := \begin{cases} \sqrt{v(1+\omega)} & \text{for } \omega \leq 0 \\ \sqrt{v(1-\omega)} & \text{for } \omega > 0. \end{cases} \tag{6}$$

The function $\hat{\psi}_2$ is shown in Fig. 3(b). Before stating a theorem about the properties of $\hat{\psi}_2$ we need the following two auxiliary lemmas. Recall that a function $f \colon \mathbb{R} \to \mathbb{R}$ is *point symmetric*

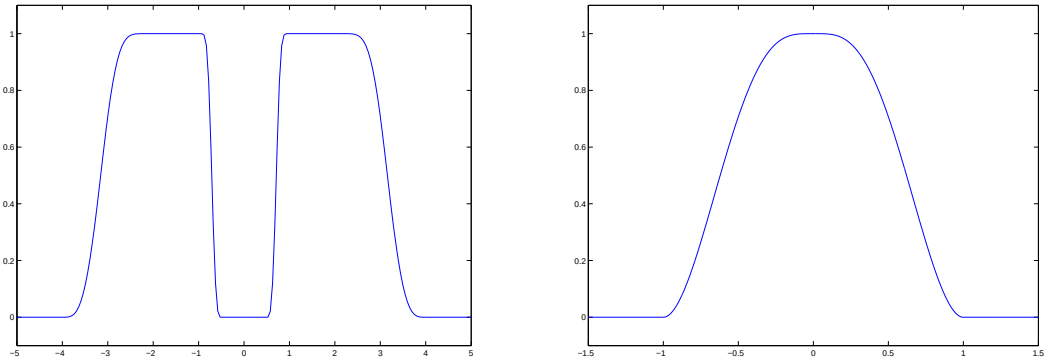

(a) $\hat{\psi}_1$ (b) $\hat{\psi}_2$

Figure 3: The functions $\hat{\psi}_1$ in (4) and $\hat{\psi}_2$ in (6)

with respect to (a, b) if and only if

$$f(a + x) - b = -f(a - x) + b \quad \forall\ x \in \mathbb{R}.$$

With the substitution $x + a \to x$ this is equivalent to

$$f(x) + f(2a - x) = 2b \quad \forall\ x \in \mathbb{R}.$$

Thus, for a function symmetric to $(0.5, 0.5)$ we have that $f(x) + f(1 - x) = 1$.

Lemma 2.3. *The function v in* (1) *is symmetric with respect to* $(0.5, 0.5)$*, i.e.,* $v(x)+v(1-x) = 1\ \forall\ x \in \mathbb{R}$.

Proof. The symmetry is obvious for $x < 0$ and $x > 1$. It remains to prove the symmetry for

$0 \leq x \leq 1$, we have

$$\begin{aligned}
&v(x) + v(1-x) \\
&= 35x^4 - 84x^5 + 70x^6 - 20x^7 + 35(1-x)^4 - 84(1-x)^5 + 70(1-x)^6 - 20(1-x)^7 \\
&= 35x^4 - 84x^5 + 70x^6 - 20x^7 \\
&+ 35\sum_{k=0}^{4}\binom{4}{k}(-x)^k - 84\sum_{k=0}^{5}\binom{5}{k}(-x)^k + 70\sum_{k=0}^{6}\binom{6}{k}(-x)^k - 20\sum_{k=0}^{7}\binom{7}{k}(-x)^k \\
&= 1.
\end{aligned}$$

□

Note that $\hat{\psi}_2$ is axially symmetric to the y-axis.

Lemma 2.4. *The function $\hat{\psi}_2$ fulfills*

$$\hat{\psi}_2^2(\omega - 1) + \hat{\psi}_2^2(\omega) + \hat{\psi}_2^2(\omega + 1) = 1 \quad \textit{for } |\omega| \leq 1.$$

Proof. We have that

$$\hat{\psi}_2^2(\omega) = \begin{cases} v(1+\omega) & \text{for } \omega \leq 0 \\ v(1-\omega) & \text{for } \omega > 0. \end{cases}$$

Consequently we get for $0 \leq \omega \leq 1$ that

$$\begin{aligned}
\hat{\psi}_2^2(\omega - 1) + \hat{\psi}_2^2(\omega) + \hat{\psi}_2^2(\omega + 1) &= v(1 + \omega - 1) + v(1 - \omega) + v(1 - \omega - 1) \\
&= v(\omega) + v(1 - \omega) + \underbrace{v(-\omega)}_{=0} \\
&= 1,
\end{aligned}$$

and similarly we obtain for $-1 \leq \omega < 0$ that

$$\begin{aligned}
\hat{\psi}_2^2(\omega - 1) + \hat{\psi}_2^2(\omega) + \hat{\psi}_2^2(\omega + 1) &= v(1 + \omega - 1) + v(1 - \omega) + v(1 - \omega - 1) \\
&= \underbrace{v(-|\omega|)}_{=0} + v(1 - |\omega|) + v(|\omega|) \\
&= 1.
\end{aligned}$$

□

As can be seen in the proof the sum reduces in both cases to two (different) summands, in particular

$$1 = \hat{\psi}_2^2(\omega - 1) + \hat{\psi}_2^2(\omega) + \hat{\psi}_2^2(\omega + 1) = \begin{cases} \hat{\psi}_2^2(\omega - 1) + \hat{\psi}_2^2(\omega) & \text{for } 0 \leq \omega \leq 1 \\ \hat{\psi}_2^2(\omega) + \hat{\psi}_2^2(\omega + 1) & \text{for } -1 \leq \omega < 0. \end{cases}$$

With these lemmas we can prove the following theorem.

Theorem 2.5. *The function $\hat{\psi}_2$ defined in* (6) *fulfills*

$$\sum_{k=-2^j}^{2^j} |\hat{\psi}_2(k+2^j\omega)|^2 = 1 \quad \textit{for } |\omega| \le 1,\ j \ge 0. \tag{7}$$

Proof. With $\widetilde{\omega} := 2^j\omega$ the assertion in (7) becomes

$$\sum_{k=-2^j}^{2^j} |\hat{\psi}_2(k+\tilde{\omega})|^2 = 1 \quad \text{for } |\tilde{\omega}| \le 2^j,\ j \ge 0.$$

For a fixed (but arbitrary) $\omega^\star \in [-2^j, 2^j] \subset \mathbb{R}$ we need that $-1 \le \omega^\star + k \le 1$ for $\hat{\psi}_2(\omega^\star + k) \neq 0$ since $\operatorname{supp}\hat{\psi}_2 = [-1,1]$. Thus, for $\omega^\star \in \mathbb{Z}$, only the summands for $k \in \{-\omega^\star - 1, -\omega^\star, -\omega^\star + 1\}$ do not vanish. But for $k = -\omega^\star \pm 1$ we have that $\omega^\star + k = \pm 1$ and $\hat{\psi}_2(\pm 1) = 0$. In this case the entire sum reduces to one summand $k = -\omega^\star$ such that

$$\sum_{k=-2^j}^{2^j} |\hat{\psi}_2(k+\omega^\star)|^2 = |\hat{\psi}_2(-\omega^\star + \omega^\star)|^2 = |\hat{\psi}_2(0)|^2 = 1.$$

If $\omega^\star \notin \mathbb{Z}$ and $\omega^\star > 0$ the only nonzero summands appear for $k \in \{\lfloor \omega^\star \rfloor, \lfloor \omega^\star \rfloor - 1\}$. Thus, with $0 < r^+ := \omega^\star - \lfloor \omega^\star \rfloor < 1$, we get

$$\sum_{k=-2^j}^{2^j} |\hat{\psi}_2(k+\omega^\star)|^2 = |\hat{\psi}_2(-\lfloor \omega^\star \rfloor + \omega^\star)|^2 + |\hat{\psi}_2(-\lfloor \omega^\star \rfloor - 1 + \omega^\star)|^2 = |\hat{\psi}_2(r^+)|^2 + |\hat{\psi}_2(1-r^+)|^2$$

which is equal to 1 by Lemma 2.4. Analogously we obtain for $\omega^\star \notin \mathbb{Z}$, $\omega^\star < 0$ that the remaining nonzero summands are those for $k \in \{\lceil \omega^\star \rceil, \lceil \omega^\star \rceil + 1\}$. With $-1 < r^- := \lceil \omega^\star \rceil + \omega^\star < 0$ we get

$$\sum_{k=-2^j}^{2^j} |\hat{\psi}_2(k+\omega^\star)|^2 = |\hat{\psi}_2(\lceil \omega^\star \rceil + \omega^\star)|^2 + |\hat{\psi}_2(\lceil \omega^\star \rceil + 1 + \omega^\star)|^2 = |\hat{\psi}_2(r^-)|^2 + |\hat{\psi}_2(1+r^-)|^2.$$

By Lemma 2.4 and since $\hat{\psi}_2(x) = \hat{\psi}_2(-x)$, we finally obtain

$$|\hat{\psi}_2(r^-)|^2 + |\hat{\psi}_2(1+r^-)|^2 = |\hat{\psi}_2(|r^-|)|^2 + |\hat{\psi}_2(1-|r^-|)|^2 = 1.$$

□

2.2 The continuous shearlet transform

For the shearlet transform we need a *scaling* (or *dilation*) *matrix* A_a and a *shear matrix* S_s defined by

$$A_a = \begin{pmatrix} a & 0 \\ 0 & \sqrt{a} \end{pmatrix},\ a \in \mathbb{R}^+, \quad S_s = \begin{pmatrix} 1 & s \\ 0 & 1 \end{pmatrix},\ s \in \mathbb{R}.$$

The *shearlets* $\psi_{a,s,t}$ emerge by dilation, shearing and translation of a function $\psi \in L_2(\mathbb{R}^2)$ as follows

$$\begin{aligned}\psi_{a,s,t}(x) :=& a^{-\frac{3}{4}}\psi(A_a^{-1}S_s^{-1}(x-t)) \\ =& a^{-\frac{3}{4}}\psi\left(\begin{pmatrix} \frac{1}{a} & -\frac{s}{a} \\ 0 & \frac{1}{\sqrt{a}} \end{pmatrix}(x-t)\right).\end{aligned} \tag{8}$$

We assume that $\hat{\psi}$ can be written as $\hat{\psi}(\omega_1,\omega_2) = \hat{\psi}_1(\omega_1)\hat{\psi}_2(\frac{\omega_2}{\omega_1})$. Consequently, we obtain for the Fourier transform

$$\begin{aligned}\hat{\psi}_{a,s,t}(\omega) &= a^{-\frac{3}{4}}\psi\left(\begin{pmatrix} \frac{1}{a} & -\frac{s}{a} \\ 0 & \frac{1}{\sqrt{a}} \end{pmatrix}(\cdot - t)\right)\hat{}(\omega) \\ &= a^{-\frac{3}{4}}e^{-2\pi i\langle\omega,t\rangle}\psi\left(\begin{pmatrix} \frac{1}{a} & -\frac{s}{a} \\ 0 & \frac{1}{\sqrt{a}} \end{pmatrix}\cdot\right)\hat{}(\omega) \\ &= a^{-\frac{3}{4}}e^{-2\pi i\langle\omega,t\rangle}(a^{-\frac{3}{2}})^{-1}\hat{\psi}\left(\begin{pmatrix} a & 0 \\ s\sqrt{a} & \sqrt{a} \end{pmatrix}\omega\right) \\ &= a^{\frac{3}{4}}e^{-2\pi i\langle\omega,t\rangle}\hat{\psi}\left(a\omega_1, \sqrt{a}(s\omega_1+\omega_2)\right) \\ &= a^{\frac{3}{4}}e^{-2\pi i\langle\omega,t\rangle}\hat{\psi}_1(a\omega_1)\,\hat{\psi}_2\left(a^{-\frac{1}{2}}\left(\frac{\omega_2}{\omega_1}+s\right)\right).\end{aligned}$$

The *shearlet transform* $\mathcal{SH}_\psi(f)$ of a function $f \in L^2(\mathbb{R})$ can now be defined as follows

$$\begin{aligned}\mathcal{SH}_\psi(f)(a,s,t) :=& \langle f, \psi_{a,s,t}\rangle \\ =& \langle \hat{f}, \hat{\psi}_{a,s,t}\rangle \\ =& \int_{\mathbb{R}^2}\hat{f}(\omega)\overline{\hat{\psi}_{a,s,t}(\omega)}d\omega \\ =& a^{\frac{3}{4}}\int_{\mathbb{R}^2}\hat{f}(\omega)\hat{\psi}_1(a\omega_1)\hat{\psi}_2\left(a^{-\frac{1}{2}}\left(\frac{\omega_2}{\omega_1}+s\right)\right)e^{2\pi i\langle\omega,t\rangle}d\omega \\ =& a^{\frac{3}{4}}\mathcal{F}^{-1}\left(\hat{f}(\omega)\hat{\psi}_1(a\omega_1)\hat{\psi}_2\left(a^{-\frac{1}{2}}\left(\frac{\omega_2}{\omega_1}+s\right)\right)\right)(t).\end{aligned}$$

The same formula can be derived by interpreting the shearlet transform as a convolution with the function $\psi_{a,s}(x) = \overline{\psi}(-A_a^{-1}S_s^{-1}x)$ and using the convolution theorem.

The shearlet transform is invertible if the function ψ fulfills the *admissibility property*

$$\int_{\mathbb{R}^2}\frac{|\hat{\psi}(\omega_1,\omega_2)|^2}{|\omega_1|^2}\,d\omega_1 d\omega_2 < \infty.$$

2.3 Shearlets on the cone

Up to now we have nothing said about the support of our shearlet ψ. We use band-limited shearlets, thus, we have compact support in the Fourier domain. In the previous section we assumed that $\hat{\psi}(\omega_1,\omega_2) = \hat{\psi}_1(\omega_1)\hat{\psi}_2(\frac{\omega_2}{\omega_1})$, where we now define ψ_1 and ψ_2 as in (4) and (6)

respectively. With the results shown for $\hat{\psi}_1$ with $|\omega_1| \geq \frac{1}{2}$ and $\hat{\psi}_2$ for $|\omega| < 1$, i.e., $|\omega_2| < |\omega_1|$, it is natural to define the area

$$\mathcal{C}^h := \{(\omega_1, \omega_2) \in \mathbb{R}^2 : |\omega_1| \geq \frac{1}{2}, |\omega_2| < |\omega_1|\}.$$

We will refer to this set as the *horizontal cone* (see Fig. 4). Analogously we define the *vertical cone* as

$$\mathcal{C}^v := \{(\omega_1, \omega_2) \in \mathbb{R}^2 : |\omega_2| \geq \frac{1}{2}, |\omega_2| > |\omega_1|\}.$$

To cover all $\mathbb{R}^2$ we define two more sets

$$\mathcal{C}^\times := \{(\omega_1, \omega_2) \in \mathbb{R}^2 : |\omega_1| \geq \frac{1}{2}, |\omega_2| \geq \frac{1}{2}, |\omega_1| = |\omega_2|\},$$
$$\mathcal{C}^0 := \{(\omega_1, \omega_2) \in \mathbb{R}^2 : |\omega_1| < 1, |\omega_2| < 1\},$$

where $\mathcal{C}^\times$ is the "intersection" (or the seam lines) of the two cones and $\mathcal{C}^0$ is the "low frequency" part. Altogether $\mathbb{R}^2 = \mathcal{C}^h \cup \mathcal{C}^v \cup \mathcal{C}^\times \cup \mathcal{C}^0$ with an overlapping domain

$$\mathcal{C}^\square := (-1, 1)^2 \setminus (-\frac{1}{2}, \frac{1}{2})^2. \tag{9}$$

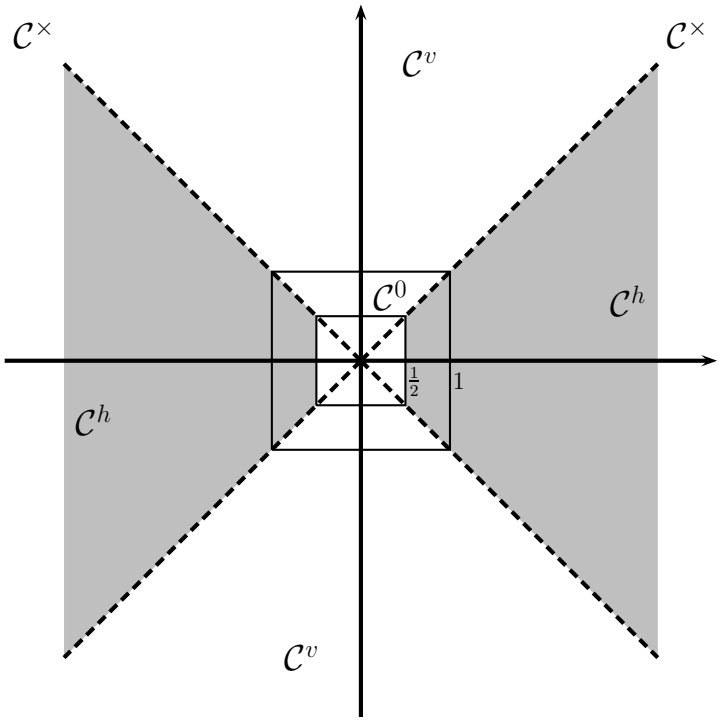

Figure 4: The sets $\mathcal{C}^h$, $\mathcal{C}^v$, $\mathcal{C}^\times$ and $\mathcal{C}^0$

Obviously the shearlet ψ defined above is perfectly suited for the horizontal cone. For each set $\mathcal{C}^\kappa$, $\kappa \in \{h, v, \times\}$, we define a characteristic function $\chi_{\mathcal{C}^\kappa}(\omega)$ which is equal to 1 for $\omega \in \mathcal{C}^\kappa$ and 0 for $\omega \notin \mathcal{C}^\kappa$. We need these characteristic functions as cut-off functions at the seam lines. We set

$$\hat{\psi}^h(\omega_1, \omega_2) := \hat{\psi}(\omega_1, \omega_2) = \hat{\psi}_1(\omega_1)\hat{\psi}_2\left(\frac{\omega_2}{\omega_1}\right)\chi_{\mathcal{C}^h}. \tag{10}$$

For the non-dilated and non-sheared $\hat{\psi}^h$ the cut-off function has no effect since the support of $\hat{\psi}^h$ is completely contained in $\mathcal{C}^h$. But after the dilation and shearing we have

$$\operatorname{supp} \hat{\psi}_{a,s,0} \subseteq \left\{ (\omega_1, \omega_2) : \frac{1}{2a} \leq |\omega_1| \leq \frac{4}{a}, \left| s + \frac{\omega_2}{\omega_1} \right| \leq \sqrt{a} \right\}.$$

The question arises for which a and s this set remains a subset of the horizontal cone. For $a > 1$ we have that $\omega_1 \leq \frac{1}{2}$ is in $\operatorname{supp} \hat{\psi}_{a,s,0}$ but not in $\mathcal{C}^h$. Thus, we can restrict ourselves to $a \leq 1$.

Having a fixed, the second condition for $\operatorname{supp} \hat{\psi}_{a,s,0}$ becomes

$$\begin{aligned} -\sqrt{a} \leq s + \frac{\omega_1}{\omega_2} &\leq \sqrt{a}, \\ -\sqrt{a} - s \leq \quad \frac{\omega_1}{\omega_2} \quad &\leq \sqrt{a} - s. \end{aligned} \tag{11}$$

Since $\left|\frac{\omega_1}{\omega_2}\right| \leq 1$ we have for the right condition $\sqrt{a} - s \leq 1$ and for the left condition $-\sqrt{a} - s \geq -1$, hence, we can conclude

$$-1 + \sqrt{a} \leq s \leq 1 - \sqrt{a}.$$

For such s we have $\operatorname{supp} \hat{\psi}_{a,s,0} \subseteq \mathcal{C}^h$, in particular the indicator function is not needed for these s (with respective a). One might ask for which s (depending on a) the indicator function cuts off only parts of the function, i.e., $\operatorname{supp} \hat{\psi}_{a,s,0} \cap \mathcal{C}^h \neq \emptyset$. We take again (11) but now we do not use a condition to *guarantee* that $\left|\frac{\omega_1}{\omega_2}\right| < 1$ but rather ask for a condition that *allows* $\left|\frac{\omega_1}{\omega_2}\right| < 1$. Thus, the right bound $\sqrt{a} - s$ should be larger than -1 and the left bound $-\sqrt{a} - s$ should be smaller than 1. Consequently, we obtain

$$-1 - \sqrt{a} \leq s \leq 1 + \sqrt{a}.$$

Summing up, we have for $|s| \leq 1 - \sqrt{a}$ that $\operatorname{supp} \hat{\psi}_{a,s,0} \subseteq \mathcal{C}^h$. For $1 - \sqrt{a} < |s| < 1 + \sqrt{a}$ parts of $\operatorname{supp} \hat{\psi}_{a,s,0}$ are also in $\mathcal{C}^v$, which are cut off. For $|s| > 1 + \sqrt{a}$ the whole shearlet is set to zero by the characteristic function. If we get back to the definition of $\hat{\psi}_{a,s,0}$ we see that the vertical range is determined by $\hat{\psi}_2$. By definition $\hat{\psi}_2$ is axially symmetric with respect to the y-axis, in other words the "center" of $\hat{\psi}_2$ is taken for the argument equal to zero, i.e., $a^{-\frac{1}{2}}(\frac{\omega_1}{\omega_2} + s) = 0$. It follows that for $|s| = 1$ the center of $\hat{\psi}_{a,s,0}$ is at the seam-lines. Thus, for $|s| = 1$ approximately one half of the shearlet is cut off whereas the other part remains. For larger s more would be cut. Consequently, we restrict ourselves to $|s| \leq 1$.

Analogously the shearlet for the vertical cone can be defined, where the roles of ω_1 and ω_2 are interchanged, i.e.,

$$\hat{\psi}^v(\omega_1, \omega_2) := \hat{\psi}(\omega_2, \omega_1) = \hat{\psi}_1(\omega_2)\hat{\psi}_2\left(\frac{\omega_1}{\omega_2}\right)\chi_{\mathcal{C}^v}. \tag{12}$$

All the results from above apply to this setting. For $(\omega_1, \omega_2) \in \mathcal{C}^\times$, i.e., $|\omega_1| = |\omega_2|$, both definitions coincide and we define

$$\hat{\psi}^\times(\omega_1, \omega_2) := \hat{\psi}(\omega_1, \omega_2)\chi_{\mathcal{C}^\times}. \tag{13}$$

The shearlets $\hat{\psi}_h$, $\hat{\psi}_v$ (and $\hat{\psi^\times}$) are called *shearlets on the cone*. This concept was introduced in [10].

We have functions to cover three of the four parts of $\mathbb{R}^2$. The remaining part $\mathcal{C}^0$ will be handled with a scaling function which is presented in the next section.

2.4 Scaling function

For the center part $\mathcal{C}^0$ (or low-frequency part) we define another set of functions. To this end, we need the following so-called "mother"-scaling function

$$\varphi(\omega) := \begin{cases} 1 & \text{for } |\omega| \leq \frac{1}{2} \\ \cos(\frac{\pi}{2} v(2|\omega| - 1)) & \text{for } \frac{1}{2} < |\omega| < 1 \\ 0 & \text{otherwise.} \end{cases}$$

The full *scaling function* ϕ can then be defined as follows

$$\begin{aligned} \hat{\phi}(\omega_1, \omega_2) &:= \begin{cases} \varphi(\omega_1) & \text{for } |\omega_1| < 1, |\omega_2| \leq |\omega_1| \\ \varphi(\omega_2) & \text{for } |\omega_2| < 1, |\omega_1| < |\omega_2| \end{cases} \\ &= \begin{cases} 1 & \text{for } |\omega_1| \leq \frac{1}{2}, |\omega_2| \leq \frac{1}{2} \\ \cos(\frac{\pi}{2} v(2|\omega_1| - 1)) & \text{for } \frac{1}{2} < |\omega_1| < 1, |\omega_2| \leq |\omega_1| \\ \cos(\frac{\pi}{2} v(2|\omega_2| - 1)) & \text{for } \frac{1}{2} < |\omega_2| < 1, |\omega_1| < |\omega_2| \\ 0 & \text{otherwise.} \end{cases} \end{aligned} \tag{14}$$

The decay of the scaling function $\hat{\phi}$ (respectively φ) is chosen to match perfectly with the increase of $\hat{\psi}_1$. For $|\omega| \in [\frac{1}{2}, 1]$ we have by (5), that

$$|\hat{\psi}_1(\omega)|^2 + |\varphi(\omega)|^2 = \sin^2\left(\frac{\pi}{2} v(2|\omega| - 1)\right) + \cos^2\left(\frac{\pi}{2} v(2|\omega| - 1)\right) = 1. \tag{15}$$

Remark 2.6. *Observe that in our setting it seems not to be useful to define the scaling function as a simple tensor product, namely*

$$\begin{aligned} \hat{\Phi}(\omega) :=& \varphi(\omega_1)\varphi(\omega_2) \\ &= \begin{cases} 1 & \textit{for } |\omega_1| \leq \frac{1}{2}, |\omega_2| \leq \frac{1}{2} \\ \cos(\frac{\pi}{2} v(2|\omega_1| - 1)) & \textit{for } \frac{1}{2} < |\omega_1| < 1, |\omega_2| \leq \frac{1}{2} \\ \cos(\frac{\pi}{2} v(2|\omega_2| - 1)) & \textit{for } \frac{1}{2} < |\omega_2| < 1, |\omega_1| \leq \frac{1}{2} \\ \cos(\frac{\pi}{2} v(2|\omega_1| - 1)) \cos(\frac{\pi}{2} v(2|\omega_2| - 1)) & \textit{for } \frac{1}{2} < |\omega_1| \leq 1, \frac{1}{2} < |\omega_2| \leq 1 \\ 0 & \textit{otherwise.} \end{cases} \end{aligned} \tag{16}$$

Fig. 5 shows the difference between both scaling functions. Obviously, the first scaling function aligns much better with the cones. Recently in [8] a new shearlet construction was introduced which is based on the scaling function in (16)*. We discuss the new construction in Section 3.4.*

Remark 2.7. *On the other hand it is possible to rewrite the definition of the original $\hat{\phi}$ as a shearlet-like tensor product. We obtain a horizontal scaling function $\hat{\phi}^h$ and a vertical scaling function $\hat{\phi}^v$ as follows*

$$\hat{\phi}^h(\omega_1, \omega_2) := \varphi(\omega_1)\varphi\left(\frac{\omega_2}{2\omega_1}\right) \quad \textit{and} \quad \hat{\phi}^v(\omega_1, \omega_2) := \varphi(\omega_2)\varphi\left(\frac{\omega_1}{2\omega_2}\right),$$

where

$$\varphi\left(\frac{\omega_2}{2\omega_1}\right) = \begin{cases} 1 & \textit{for } |\omega_2| \leq |\omega_1| \\ \cos\left(\frac{\pi}{2} v\left(\left|\frac{\omega_2}{\omega_1}\right| - 1\right)\right) & \textit{for } |\omega_1| < |\omega_2| < 2|\omega_1| \\ 0 & \textit{otherwise.} \end{cases}$$

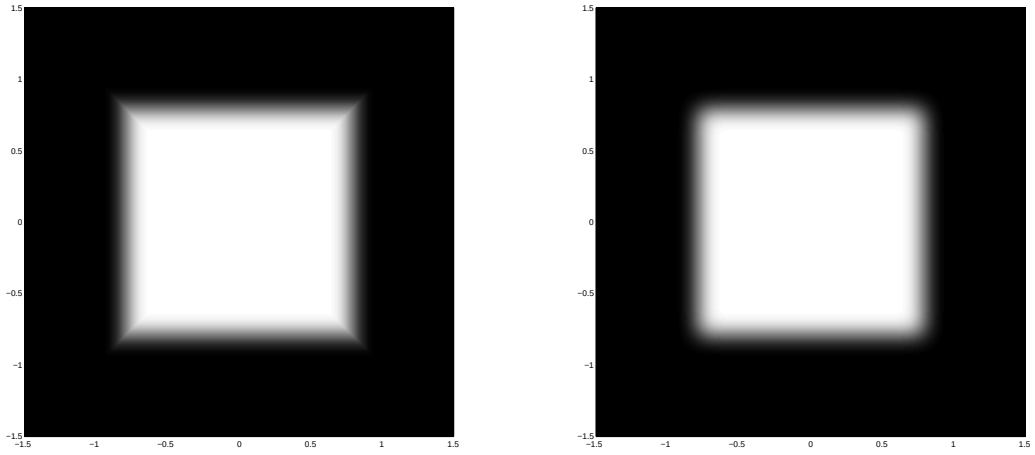

(a) $\hat{\phi}(\omega)$ (b) $\hat{\Phi}(\omega)$

Figure 5: The different scaling functions in (14) and (16).

Thus, $\varphi(\frac{\omega_2}{2\omega_1})$ is a continuous extension of the characteristic function of the horizontal cone $\mathcal{C}^h$.

We set

$$\phi_{a,s,t}(x) = \phi_t(x) = \phi(x - t).$$

Note that there is neither scaling nor shearing for the scaling function, only a translation. Thus, the index "a, s, t" from the shearlet ψ reduces to "t". We further obtain

$$\hat{\phi}_t(\omega) = e^{-2\pi i \langle \omega, t \rangle} \hat{\phi}(\omega).$$

The transform can be obtained similar as before, namely

$$\mathcal{SH}_\phi(f)(a, s, t) = \langle f, \phi_t \rangle.$$

3 Computation of the shearlet transform

In the following, we consider digital images as functions sampled on the grid $\{(\frac{m_1}{M}, \frac{m_2}{N}) : (m_1, m_2) \in \mathcal{I}\}$ with $\mathcal{I} := \{(m_1, m_2) : m_1 = 0, \ldots, M-1,\ m_2 = 0, \ldots N-1\}$.

The discrete shearlet transform is basically known, but in contrast to the existing literature we present here a fully discrete setting. That is, we do not only discretize the involved parameters a, s and t but also consider only a finite number of discrete translations t. Additionally, our setting discretizes the translation parameter t on a rectangular grid and independent of the dilation and shearing parameter. See Section 3.9 for further remarks on this topic.

3.1 Finite discrete shearlets

Let $j_0 := \lfloor \frac{1}{2} \log_2 N \rfloor$ be the number of considered scales. To obtain a discrete shearlet transform, we discretize the scaling, shear and translation parameters as

$$\begin{aligned} a_j &:= 2^{-2j} = \frac{1}{4^j}, \quad j = 0, \dots, j_0 - 1, \\ s_{j,k} &:= k 2^{-j}, \quad -2^j \le k \le 2^j, \\ t_m &:= \left(\frac{m_1}{M}, \frac{m_2}{N} \right), \quad m \in \mathcal{I}. \end{aligned} \tag{17}$$

With these notations our shearlets becomes $\psi_{j,k,m}(x) := \psi_{a_j, s_{j,k}, t_m}(x) = \psi(A_{a_j}^{-1} S_{s_{j,k}}^{-1}(x - t_m))$. Observe that compared to the continuous shearlets defined in (8) we omit the factor $a^{-\frac{3}{4}}$. In the Fourier domain we obtain

$$\hat{\psi}_{j,k,m}(\omega) = \hat{\psi}(A_{a_j}^{\mathrm{T}} S_{s_{j,k}}^{\mathrm{T}} \omega) e^{-2\pi i \langle \omega, t_m \rangle} = \hat{\psi}_1 \left(4^{-j} \omega_1 \right) \hat{\psi}_2 \left(2^j \frac{\omega_2}{\omega_1} + k \right) e^{-2\pi i \langle \omega, \binom{m_1/M}{m_2/N} \rangle}, \quad \omega \in \Omega,$$

where $\Omega := \left\{ (\omega_1, \omega_2) : \omega_1 = -\left\lfloor \frac{M}{2} \right\rfloor, \dots, \left\lceil \frac{M}{2} \right\rceil - 1,\ \omega_2 = -\left\lfloor \frac{N}{2} \right\rfloor, \dots, \left\lceil \frac{N}{2} \right\rceil - 1 \right\}$.

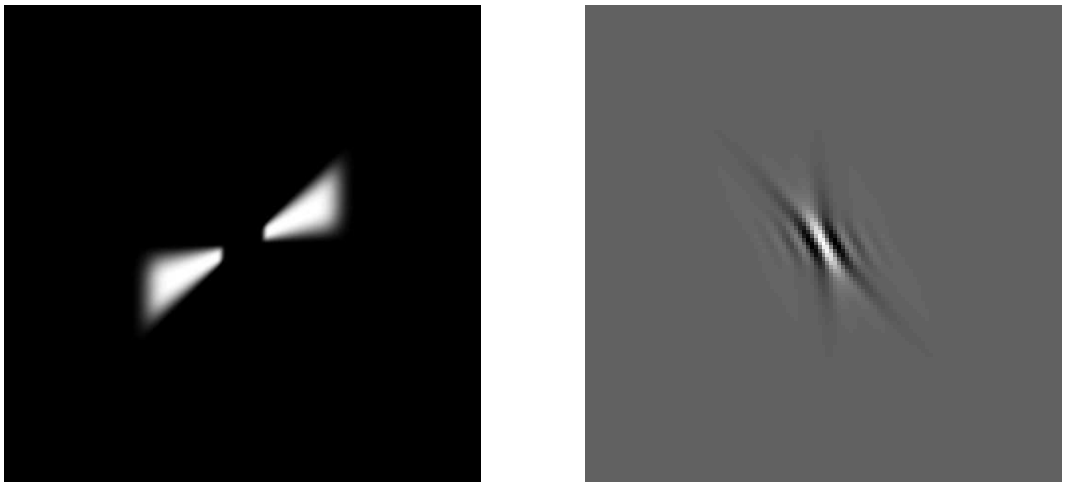

(a) Shearlet in Fourier domain for $a = \frac{1}{4}$ and $s = -\frac{1}{2}$

(b) Same shearlet in time domain (zoomed)

Figure 6: Shearlet in Fourier and time domain.

By definition we have $a \le 1$ and $|s| \le 1$. Therefore we see that we have a cut off due to the cone boundaries only for $|k| = 2^j$ where $|s| = 1$. For both cones we have for $|s| = 1$ two "half" shearlets with a gap at the seam line. None of the shearlets are defined on the seam line $\mathcal{C}^{\times}$. To obtain "full" shearlets at the seam lines we "glue" the three parts together, thus, we define for $|k| = 2^j$ a sum of shearlets

$$\hat{\psi}_{j,k,m}^{h \times v} := \hat{\psi}_{j,k,m}^{h} + \hat{\psi}_{j,k,m}^{v} + \hat{\psi}_{j,k,m}^{\times}.$$

We define the *discrete shearlet transform* as

$$\mathcal{SH}(f)(\kappa,j,k,m) := \begin{cases} \langle f, \phi_m\rangle & \text{for } \kappa = 0, \\ \langle f, \psi^{\kappa}_{j,k,m}\rangle & \text{for } \kappa \in \{h,v\}, \\ \langle f, \psi^{h\times v}_{j,k,m}\rangle & \text{for } \kappa = \times, |k| = 2^j. \end{cases}$$

where $j = 0,\dots,j_0-1$, $-2^j+1 \le k \le 2^j-1$ and $m \in \mathcal{I}$ if not stated in another way. The shearlet transform can be efficiently realized by applying the `fft2` and its inverse `ifft2` which compute the following discrete Fourier transforms with $\mathcal{O}(N^2 \log N)$ arithmetic operations:

$$\begin{aligned} \hat{f}(\omega) &= \sum_{m\in\mathcal{I}} f(m) e^{-2\pi i \left\langle \omega, \binom{m_1/M}{m_2/N}\right\rangle} = \sum_{m\in\mathcal{I}} f(m) e^{-2\pi i\left(\frac{\omega_1 m_1}{M}+\frac{\omega_2 m_2}{N}\right)}, \quad \omega \in \Omega, \\ f(m) &= \frac{1}{MN}\sum_{\omega\in\Omega} \hat{f}(\omega) e^{2\pi i \left\langle \omega, \binom{m_1/M}{m_2/N}\right\rangle} = \frac{1}{MN}\sum_{\omega\in\Omega} \hat{f}(\omega) e^{2\pi i\left(\frac{\omega_1 m_1}{M}+\frac{\omega_2 m_2}{N}\right)}, \quad m \in \mathcal{I}. \end{aligned}$$

We have the Plancherel formula

$$\langle f, g\rangle = \frac{1}{MN}\langle \hat{f}, \hat{g}\rangle.$$

Thus, the discrete shearlet transform can be computed for $\kappa = h$ as follows (observe that $\hat{\psi}$ is real):

$$\begin{aligned} \mathcal{SH}(f)(h,j,k,m) &= \langle f, \psi^h_{j,k,m}\rangle = \frac{1}{MN}\langle \hat{f}, \hat{\psi}^h_{j,k,m}\rangle \\ &= \frac{1}{MN}\sum_{\omega\in\Omega} \overline{e^{-2\pi i\langle \omega, \binom{m_1/M}{m_2/N}\rangle}\hat{\psi}(4^{-j}\omega_1, 4^{-j}k\omega_1 + 2^{-j}\omega_2)}\hat{f}(\omega_1,\omega_2) \\ &= \frac{1}{MN}\sum_{\omega\in\Omega} \hat{\psi}(4^{-j}\omega_1, 4^{-j}k\omega_1 + 2^{-j}\omega_2)\hat{f}(\omega_1,\omega_2) e^{2\pi i\left\langle \omega, \binom{m_1/M}{m_2/N}\right\rangle}. \end{aligned}$$

With $\hat{g}_{j,k}(\omega) := \hat{\psi}(4^{-j}\omega_1, 4^{-j}k\omega_1 + 2^{-j}\omega_2)\hat{f}(\omega_1,\omega_2)$ this can be rewritten as

$$\mathcal{SH}(f)(h,j,k,m) = \frac{1}{MN}\sum_{\omega\in\Omega} \hat{g}_{j,k}(\omega) e^{2\pi i\left\langle \omega, \binom{m_1/M}{m_2/N}\right\rangle}.$$

Since $\hat{g}_{j,k}(\omega) \in \mathbb{C}^{M\times N}$ the shearlet transform can be computed as an inverse FFT of $\hat{g}_{j,k}$, thus

$$\begin{aligned} \mathcal{SH}(f)(h,j,k,m) &= \texttt{ifft2}(\hat{g}_{j,k}) \\ &= \texttt{ifft2}(\hat{\psi}(4^{-j}\omega_1, 4^{-j}k\omega_1 + 2^{-j}\omega_2)\hat{f}(\omega_1,\omega_2)). \end{aligned} \tag{18}$$

For the vertical cone, i.e., $\kappa = v$, we obtain

$$\mathcal{SH}(f)(v,j,k,m) = \texttt{ifft2}(\hat{\psi}(4^{-j}\omega_2, 4^{-j}k\omega_2 + 2^{-j}\omega_1)\hat{f}(\omega_1,\omega_2)) \tag{19}$$

and for the seam line part with $|k| = 2^j$ we use the "glued" shearlets and obtain

$$\mathcal{SH}(f)_{\psi^{h\times v}}(j,k,m) = \texttt{ifft2}(\hat{\psi}^{h\times v}(4^{-j}\omega_1, 4^{-j}k\omega_1 + 2^{-j}\omega_2)\hat{f}(\omega_1,\omega_2)). \tag{20}$$

Finally for the low-pass with $\hat{g}_0(\omega_1,\omega_2) := \hat{\phi}(\omega_1,\omega_2)\hat{f}(\omega_1,\omega_2)$ the transform can be obtained similar as before, namely

$$\begin{aligned}
\mathcal{SH}_\phi(f)(m) &= \langle f, \phi_m\rangle \\
&= \frac{1}{MN}\langle \hat{f}, \hat{\phi}_m\rangle \\
&= \frac{1}{MN}\sum_{\omega\in\Omega} \overline{e^{-2\pi i\langle \omega, \binom{m_1/M}{m_2/N}\rangle}\hat{\phi}(\omega_1,\omega_2)}\hat{f}(\omega_1,\omega_2) \\
&= \frac{1}{MN}\sum_{\omega\in\Omega} e^{+2\pi i\langle \omega, \binom{m_1/M}{m_2/N}\rangle}\hat{\phi}(\omega_1,\omega_2)\hat{f}(\omega_1,\omega_2) \\
&= \frac{1}{MN}\sum_{\omega\in\Omega} e^{+2\pi i\langle \omega, \binom{m_1/M}{m_2/N}\rangle}\hat{g}_0(\omega) \\
&= \texttt{ifft2}(\hat{g}_0) \\
&= \texttt{ifft2}(\hat{\phi}(\omega_1,\omega_2)\hat{f}(\omega_1,\omega_2)). \qquad (21)
\end{aligned}$$

The complete shearlet transform is the combination of (18) to (21). We summarize

$$\mathcal{SH}(f)(\kappa,j,k,m) = \begin{cases} \texttt{ifft2}(\hat{\phi}(\omega_1,\omega_2)\hat{f}(\omega_1,\omega_2)) & \text{for } \kappa = 0 \\ \texttt{ifft2}(\hat{\psi}(4^{-j}\omega_1, 4^{-j}k\omega_1 + 2^{-j}\omega_2)\hat{f}(\omega_1,\omega_2)) & \text{for } \kappa = h, |k| \le 2^j - 1 \\ \texttt{ifft2}(\hat{\psi}(4^{-j}\omega_2, 4^{-j}k\omega_2 + 2^{-j}\omega_1)\hat{f}(\omega_1,\omega_2)) & \text{for } \kappa = v, |k| \le 2^j - 1 \\ \texttt{ifft2}(\hat{\psi}^{h\times v}(4^{-j}\omega_1, 4^{-j}k\omega_1 + 2^{-j}\omega_2)\hat{f}(\omega_1,\omega_2)) & \text{for } \kappa \neq 0, |k| = 2^j. \end{cases} \qquad (22)$$

3.2 A discrete shearlet frame

In view of the inverse shearlet transform we prove that our discrete shearlets constitute a Parseval frame of the finite Euclidean space $L_2(\mathcal{I})$. Recall that for a Hilbert space $\mathcal{H}$ a sequence $\{u_j : j \in \mathcal{J}\}$ is a *frame* if and only if constants $0 < A \le B < \infty$ exists such that

$$A\|f\|^2 \le \sum_{j\in\mathcal{J}} |\langle f, u_j\rangle|^2 \le B\|f\|^2 \quad \text{for all } f \in \mathcal{H}.$$

The frame is called *tight* if $A = B$ and a *Parseval* frame if $A = B = 1$. Thus, for Parseval frames we have that

$$\|f\|^2 = \sum_{j\in\mathcal{J}} |\langle f, u_j\rangle|^2 \quad \text{for all } f \in \mathcal{H}$$

which is equivalent to the reconstruction formula

$$f = \sum_{j\in\mathcal{J}} \langle f, u_j\rangle u_j \quad \text{for all } f \in \mathcal{H}.$$

Further details on frames can be found in [3] and [14]. In the n-dimensional Euclidean space we can arrange the frame elements u_j, $j = 1,\dots,\tilde{n} \ge n$ as rows of a matrix U. Then we have indeed a frame if U has full rank and a Parseval frame if and only if $U^{\mathrm{T}}U = I_n$. Note that

$UU^{\mathrm{T}} = I_{\tilde{n}}$ is only true if the frame is an orthonormal basis. The Parseval frame transform and its inverse read

$$(\langle f, u_j\rangle)_{j=1}^{\tilde{n}} = Uf \quad \text{and} \quad f = U^{\mathrm{T}}(\langle f, u_j\rangle)_{j=1}^{\tilde{n}}.$$

By the following theorem our shearlets provide such a convenient system.

Theorem 3.1. *The discrete shearlet system*

$$\begin{aligned}
&\{\psi^h_{j,k,m}(\omega) : j = 0, \dots, j_0 - 1, -2^j + 1 \le k \le 2^j - 1, m \in \mathcal{I}\}\\
&\cup \{\psi^v_{j,k,m}(\omega) : j = 0, \dots, j_0 - 1, -2^j + 1 \le k \le 2^j - 1, m \in \mathcal{I}\}\\
&\cup \{\psi^{h\times v}_{j,k,m}(\omega) : j = 0, \dots, j_0 - 1, |k| = 2^j, m \in \mathcal{I}\}\\
&\cup \{\phi_m(\omega) : m \in \mathcal{I}\}
\end{aligned}$$

provides a Parseval frame for $L^2(\mathcal{I})$.

Proof. We have to show that

$$\|f\|^2 = \sum_{\kappa\in\{h,v\}} \sum_{j=0}^{j_0-1} \sum_{k=-2^j+1}^{2^j-1} \sum_{m\in\mathcal{I}} |\langle f, \psi^\kappa_{j,k,m}\rangle|^2 + \sum_{j=0}^{j_0-1} \sum_{k=\pm 2^j} \sum_{m\in\mathcal{I}} |\langle f, \psi^{h\times v}_{j,k,m}\rangle|^2 + \sum_{m\in\mathcal{I}} |\langle f, \phi_m\rangle|^2 =: C.$$

Since $\|f\|_F^2 = \frac{1}{MN}\|\hat{f}\|_F^2$ (Parsevals formula, $\|\cdot\|$ denotes the Frobenius norm, i.e., $\|\cdot\|_F = \|\mathrm{vec}(\cdot)\|_2$) it is sufficient to show that C is equal to $\frac{1}{MN}\|\hat{f}\|_F^2$.

By (18) we know that

$$\langle f, \psi^h_{j,k,m}\rangle = \frac{1}{MN} \sum_{\omega\in\Omega} e^{2\pi i \langle \omega, \binom{m_1/M}{m_2/N}\rangle} \hat{g}_{j,k}(\omega) = g_{j,k}(m).$$

We further obtain

$$\sum_{m\in\mathcal{I}} |\langle f, \psi^h_{j,k,m}\rangle|^2 = \sum_{m\in\mathcal{I}} |g_{j,k}(m)|^2 = \|g_{j,k}\|_F^2.$$

Consequently, with Parsevals formula

$$\begin{aligned}
\|g_{j,k}\|_F^2 &= \frac{1}{MN}\|\hat{g}_{j,k}\|_F^2 = \frac{1}{MN} \sum_{\omega\in\Omega} |\hat{g}_{j,k}(\omega)|^2\\
&= \frac{1}{MN} \sum_{\omega\in\Omega} |\hat{\psi}(4^{-j}\omega_1, 4^{-j}k\omega_1 + 2^{-j}\omega_2)\hat{f}(\omega_1, \omega_2)|^2\\
&= \frac{1}{MN} \sum_{\omega\in\Omega} |\hat{\psi}(4^{-j}\omega_1, 4^{-j}k\omega_1 + 2^{-j}\omega_2)|^2 |\hat{f}(\omega_1, \omega_2)|^2.
\end{aligned}$$

Analogously we obtain for the vertical part

$$\sum_{m\in\mathcal{I}} |\langle f, \psi^v_{j,k,m}\rangle|^2 = \frac{1}{MN} \sum_{\omega\in\Omega} |\hat{\psi}(4^{-j}\omega_2, 4^{-j}k\omega_2 + 2^{-j}\omega_1)|^2 |\hat{f}(\omega_1, \omega_2)|^2.$$

Using these results we can conclude for the seam-line part

$$\begin{aligned}\sum_{m\in\mathcal{I}} |\langle f, \psi^{h\times v}_{j,k,m}\rangle|^2 &= \frac{1}{MN}\sum_{\omega\in\Omega} |\hat{\psi}(4^{-j}\omega_1, 4^{-j}k\omega_1 + 2^{-j}\omega_2)|^2 |\hat{f}(\omega_1,\omega_2)|^2 \chi_{\mathcal{C}^h} \\ &+ \frac{1}{MN}\sum_{\omega\in\Omega} |\hat{\psi}(4^{-j}\omega_2, 4^{-j}k\omega_2 + 2^{-j}\omega_1)|^2 |\hat{f}(\omega_1,\omega_2)|^2 \chi_{\mathcal{C}^v} \\ &+ \frac{1}{MN}\sum_{\omega\in\Omega} |\hat{\psi}(4^{-j}\omega_1, 4^{-j}k\omega_1 + 2^{-j}\omega_2)|^2 |\hat{f}(\omega_1,\omega_2)|^2 \chi_{\mathcal{C}^\times}.\end{aligned}$$

For the remaining low-pass part we get similarly

$$\begin{aligned}\sum_{m\in\mathcal{I}} |\langle f, \phi_m\rangle|^2 &= \frac{1}{MN}\sum_{m\in\mathcal{I}} |\langle \hat{f}, \hat{\phi}_m\rangle|^2 \\ &= \frac{1}{MN}\sum_{m\in\mathcal{I}} \Big|\sum_{\omega\in\Omega} \overline{\hat{\phi}_m(\omega)}\hat{f}(\omega)\Big|^2 \\ &= \frac{1}{MN}\sum_{m\in\Omega} \Big|\sum_{\omega\in\Omega} e^{2\pi i\langle \omega, \binom{m_1/M}{m_2/N}\rangle}\hat{\phi}(\omega_1,\omega_2)\hat{f}(\omega_1,\omega_2)\Big|^2\end{aligned}$$

with $\hat{g}_0(\omega) := \hat{\phi}(\omega_1,\omega_2)\hat{f}(\omega_1,\omega_2)$

$$\begin{aligned}&= \sum_{m\in\mathcal{I}} \Big|\frac{1}{MN}\sum_{\omega\in\Omega} e^{2\pi i\langle \omega, \binom{m_1/M}{m_2/N}\rangle}\hat{g}_0(\omega)\Big|^2 \\ &= \sum_{m\in\mathcal{I}} |g_0(m)|^2 = \|g_0\|_F^2 = \frac{1}{MN}\|\hat{g}_0\|^2 \\ &= \frac{1}{MN}\sum_{\omega\in\Omega} |\hat{\phi}(\omega_1,\omega_2)\hat{f}(\omega_1,\omega_2)|^2 \\ &= \frac{1}{MN}\sum_{\omega\in\Omega} |\hat{\phi}(\omega_1,\omega_2)|^2 |\hat{f}(\omega_1,\omega_2)|^2.\end{aligned}$$

Lets put the pieces together:

$$
\begin{aligned}
C &= \sum_{\kappa\in\{h,v\}}\sum_{j=0}^{j_0-1}\sum_{k=-2^j+1}^{2^j-1}\sum_{m\in\mathcal{I}}|\langle f,\psi^{\kappa}_{j,k,m}\rangle|^2+\sum_{j=0}^{j_0-1}\sum_{k=\pm 2^j}\sum_{m\in\mathcal{I}}|\langle f,\psi^{h\times v}_{j,k,m}\rangle|^2+\sum_{m\in\mathcal{I}}|\langle f,\phi_m\rangle|^2\\
&=\sum_{j=0}^{j_0-1}\sum_{k=-2^j+1}^{2^j-1}\frac{1}{MN}\sum_{\omega\in\Omega}|\hat{\psi}(4^{-j}\omega_1,4^{-j}k\omega_1+2^{-j}\omega_2)|^2|\hat{f}(\omega_1,\omega_2)|^2\\
&\quad+\sum_{j=0}^{j_0-1}\sum_{k=-2^j+1}^{2^j-1}\frac{1}{MN}\sum_{\omega\in\Omega}|\hat{\psi}(4^{-j}\omega_2,4^{-j}k\omega_2+2^{-j}\omega_1)|^2|\hat{f}(\omega_1,\omega_2)|^2\\
&\quad+\sum_{j=0}^{j_0-1}\sum_{k=\pm 2^j}\Bigg(\frac{1}{MN}\sum_{\omega\in\Omega}|\hat{\psi}(4^{-j}\omega_1,4^{-j}k\omega_1+2^{-j}\omega_2)|^2|\hat{f}(\omega_1,\omega_2)|^2\chi_{\mathcal{C}^h}\\
&\quad+\frac{1}{MN}\sum_{\omega\in\Omega}|\hat{\psi}(4^{-j}\omega_2,4^{-j}k\omega_2+2^{-j}\omega_1)|^2|\hat{f}(\omega_1,\omega_2)|^2\chi_{\mathcal{C}^v}\\
&\quad+\frac{1}{MN}\sum_{\omega\in\Omega}|\hat{\psi}(4^{-j}\omega_1,4^{-j}k\omega_1+2^{-j}\omega_2)|^2|\hat{f}(\omega_1,\omega_2)|^2\chi_{\mathcal{C}^\times}\Bigg)\\
&\quad+\frac{1}{MN}\sum_{\omega\in\Omega}|\hat{\phi}(\omega_1,\omega_2)|^2|\hat{f}(\omega_1,\omega_2)|^2.
\end{aligned}
$$

We can group the sums by the different sets and obtain

$$
\begin{aligned}
C &= \frac{1}{MN}\sum_{\omega\in\Omega}\sum_{j=0}^{j_0-1}\sum_{k=-2^j}^{2^j}|\hat{\psi}(4^{-j}\omega_1,4^{-j}k\omega_1+2^{-j}\omega_2)|^2|\hat{f}(\omega_1,\omega_2)|^2\chi_{\mathcal{C}^h}\\
&\quad+\frac{1}{MN}\sum_{\omega\in\Omega}\sum_{j=0}^{j_0-1}\sum_{k=-2^j}^{2^j}|\hat{\psi}(4^{-j}\omega_2,4^{-j}k\omega_2+2^{-j}\omega_1)|^2|\hat{f}(\omega_1,\omega_2)|^2\chi_{\mathcal{C}^v}\\
&\quad+\frac{1}{MN}\sum_{\omega\in\Omega}\sum_{j=0}^{j_0-1}|\hat{f}(\omega_1,\omega_2)|^2|\underbrace{\hat{\psi}(4^{-j}\omega_1,0)}_{=1}|^2\chi_{\mathcal{C}^\times}+\frac{1}{MN}\sum_{\omega\in\Omega}|\hat{\phi}(\omega_1,\omega_2)|^2|\hat{f}(\omega_1,\omega_2)|^2.
\end{aligned}
$$

Using the definition of $\hat{\psi}$ in (10) (or (12) and (13), respectively), we can conclude

$$
\begin{aligned}
C &= \frac{1}{MN}\sum_{\omega\in\mathcal{C}^h}|\hat{f}(\omega_1,\omega_2)|^2\underbrace{\sum_{j=0}^{j_0-1}|\hat{\psi}_1(4^{-j}\omega_1)|^2}_{\substack{=1\text{ for }|\omega_1|\geq 1\\(\text{see Theorem 2.2})}}\underbrace{\sum_{k=-2^j}^{2^j}|\hat{\psi}_2(2^j\frac{\omega_2}{\omega_1}+k)|^2}_{=1\text{ (see Theorem 2.5)}}\\
&\quad+\frac{1}{MN}\sum_{\omega\in\mathcal{C}^v}|\hat{f}(\omega_1,\omega_2)|^2\underbrace{\sum_{j=0}^{j_0-1}|\hat{\psi}_1(4^{-j}\omega_2)|^2}_{=1\text{ for }|\omega_2|\geq 1}\underbrace{\sum_{k=-2^j}^{2^j}|\hat{\psi}_2(2^j\frac{\omega_1}{\omega_2}+k)|^2}_{=1}\\
&\quad+\frac{1}{MN}\sum_{\omega\in\mathcal{C}^\times}|\hat{f}(\omega_1,\omega_2)|^2+\frac{1}{MN}\sum_{\omega\in\Omega}|\underbrace{\hat{\phi}(\omega_1,\omega_2)}_{=1\text{ for }\omega\in[-\frac{1}{2},\frac{1}{2}]^2}|^2|\hat{f}(\omega_1,\omega_2)|^2.
\end{aligned}
$$

With the properties of $\hat{\psi}_1$ and $\hat{\psi}_2$ (see Theorems 2.2 and 2.5) we obtain two sums, one for the overlapping domain $\mathcal{C}^\square$ (see (9)) and one for the remaining part

$$C = \frac{1}{MN} \sum_{\omega \in \Omega \setminus \mathcal{C}^\square} |\hat{f}(\omega_1, \omega_2)|^2 + \sum_{\omega \in \mathcal{C}^\square} |\hat{f}(\omega_1, \omega_2)|^2 \left(\sum_{j=0}^{j_0-1} |\hat{\psi}_1(4^{-j}\omega_1)|^2 + \sum_{j=0}^{j_0-1} |\hat{\psi}_1(4^{-j}\omega_2)|^2 + |\hat{\phi}(\omega_1, \omega_2)|^2 \right)$$

where we can split up the second sum as

$$\begin{aligned} C = & \frac{1}{MN} \sum_{\omega \in \Omega \setminus \mathcal{C}^\square} |\hat{f}(\omega_1, \omega_2)|^2 \\ & + \frac{1}{MN} \sum_{\omega \in \mathcal{C}^h \cap \mathcal{C}^\square} |\hat{f}(\omega_1, \omega_2)|^2 \sin^2\left(\frac{\pi}{2} v(2|\omega_1| - 1)\right) + \frac{1}{MN} \sum_{\omega \in \mathcal{C}^v \cap \mathcal{C}^\square} |\hat{f}(\omega_1, \omega_2)|^2 \sin^2\left(\frac{\pi}{2} v(2|\omega_2| - 1)\right) \\ & + \frac{1}{MN} \sum_{\omega \in \mathcal{C}^h \cap \mathcal{C}^\square} |\hat{f}(\omega_1, \omega_2)|^2 \cos^2\left(\frac{\pi}{2} v(2|\omega_1| - 1)\right) + \frac{1}{MN} \sum_{\omega \in \mathcal{C}^v \cap \mathcal{C}^\square} |\hat{f}(\omega_1, \omega_2)|^2 \cos^2\left(\frac{\pi}{2} v(2|\omega_2| - 1)\right) \end{aligned}$$

using the overlap (see (15)) we can continue

$$\begin{aligned} C = & \frac{1}{MN} \sum_{\omega \in \Omega \setminus \mathcal{C}^\square} |\hat{f}(\omega_1, \omega_2)|^2 \\ & + \frac{1}{MN} \sum_{\omega \in \mathcal{C}^h \cap \mathcal{C}^\square} |\hat{f}(\omega_1, \omega_2)|^2 \underbrace{\left(\sin^2\left(\frac{\pi}{2} v(2|\omega_1| - 1)\right) + \cos^2\left(\frac{\pi}{2} v(2|\omega_1| - 1)\right) \right)}_{=1 \text{ (see (15))}} \\ & + \frac{1}{MN} \sum_{\omega \in \mathcal{C}^v \cap \mathcal{C}^\square} |\hat{f}(\omega_1, \omega_2)|^2 \underbrace{\left(\sin^2\left(\frac{\pi}{2} v(2|\omega_2| - 1)\right) + \cos^2\left(\frac{\pi}{2} v(2|\omega_2| - 1)\right) \right)}_{=1 \text{ (see (15))}}. \end{aligned}$$

Finally, we obtain

$$C = \frac{1}{MN} \sum_{\omega \in \Omega} |\hat{f}(\omega_1, \omega_2)|^2 = \frac{1}{MN} \|\hat{f}\|_F^2 = \|f\|_F^2.$$

□

3.3 Inversion of the shearlet transform

Having the discrete Parseval frame the inversion of the shearlet transform is straightforward: multiply each coefficient with the respective shearlet and sum over all involved parameters. As an inversion formula we obtain

$$f = \sum_{\kappa \in \{h,v\}} \sum_{j=0}^{j_0-1} \sum_{k=-2^j+1}^{2^j-1} \sum_{m \in \mathcal{I}} \langle f, \psi_{j,k,m}^\kappa \rangle \psi_{j,k,m}^\kappa + \sum_{j=0}^{j_0-1} \sum_{k=\pm 2^j} \sum_{m \in \mathcal{I}} \langle f, \psi_{j,k,m}^{h \times v} \rangle \psi_{j,k,m}^{h \times v} + \sum_{m \in \mathcal{I}} \langle f, \phi_m \rangle \phi_m.$$

The actual computation of f from given coefficients $c(\kappa, j, k, m)$ is done in the Fourier domain. Due to the linearity of the Fourier transform we get

$$\hat{f} = \sum_{\kappa \in \{h,v\}} \sum_{j=0}^{j_0-1} \sum_{k=-2^j+1}^{2^j-1} \sum_{m \in \mathcal{I}} \langle f, \psi_{j,k,m}^\kappa \rangle \hat{\psi}_{j,k,m}^\kappa + \sum_{j=0}^{j_0-1} \sum_{k=\pm 2^j} \sum_{m \in \mathcal{I}} \langle f, \psi_{j,k,m}^{h \times v} \rangle \hat{\psi}_{j,k,m}^{h \times v} + \sum_{m \in \mathcal{I}} \langle f, \phi_m \rangle \hat{\phi}_m.$$

We take a closer look at the part for the horizontal cone where we have

$$\begin{aligned}\hat{f}(\omega)\chi_{\mathcal{C}^h} &= \sum_{j=0}^{j_0-1}\sum_{k=-2^j+1}^{2^j-1}\sum_{m\in\mathcal{I}}\langle f,\psi_{j,k,m}\rangle\hat{\psi}^h_{j,k,m}(\omega)\\ &= \sum_{j=0}^{j_0-1}\sum_{k=-2^j+1}^{2^j-1}\sum_{m\in\mathcal{I}} c(h,j,k,m)e^{-2\pi i\langle\omega,\binom{m_1/M}{m_2/N}\rangle}\hat{\psi}(4^{-j}\omega_1, 4^j k\omega_1 + 2^{-j}\omega_2).\end{aligned}$$

The inner sum can be interpreted as a two-dimensional discrete Fourier transform and can be computed with a FFT and we can write

$$\hat{f}(\omega)\chi_{\mathcal{C}^h} = \sum_{j=0}^{j_0-1}\sum_{k=-2^j+1}^{2^j-1} \texttt{fft2}(c(h,j,k,\cdot))(\omega_1,\omega_2)\hat{\psi}(4^{-j}\omega_1, 4^j k\omega_1 + 2^{-j}\omega_2).$$

Hence, $\hat{f}$ can be computed by simple multiplications of the Fourier-transformed shearlet coefficients with the dilated and sheared spectra of ψ and afterwards summing over all "parts", scales j and all shears k, respectively. In detail we have

$$\begin{aligned}\hat{f}(\omega_1,\omega_2) =& \texttt{fft2}(c(0,\cdot))\hat{\phi}(\omega_1,\omega_2)\\ &+\sum_{j=0}^{j_0-1}\sum_{k=-2^j+1}^{2^j-1} \texttt{fft2}(c(h,j,k,\cdot))\hat{\psi}(4^{-j}\omega_1, 4^{-j}k\omega_1 + 2^{-j}\omega_2)\\ &+\sum_{j=0}^{j_0-1}\sum_{k=-2^j+1}^{2^j-1} \texttt{fft2}(c(v,j,k,\cdot))\hat{\psi}(4^{-j}\omega_2, 4^{-j}k\omega_2 + 2^{-j}\omega_1)\\ &+\sum_{j=0}^{j_0-1}\sum_{k=\pm 2^j} \texttt{fft2}(c(h\times v,j,k,\cdot))\hat{\psi}(4^{-j}\omega_1, 4^{-j}k\omega_1 + 2^{-j}\omega_2).\end{aligned} \tag{23}$$

Finally we get f itself by an iFFT of $\hat{f}$

$$f = \texttt{ifft2}(\hat{f}).$$

3.4 Smooth shearlets

In many theoretical and some practical purposes one needs smooth shearlets in the Fourier domain because such shearlets provide well-localized shearlets in time domain. Recently, in [8] a new shearlet construction was proposed that provides smooth shearlets for all scales a and respective shears s. Our shearlets are smooth for all scales and for all shears $|s| \neq 1$. The "diagonal" shearlets $\psi^{h\times v}$ are continuous by construction but they are not smooth. Fig 7(a) illustrates this. Obviously our construction is not smooth in points on the diagonal. The new construction circumvents this with "round" corners. To this end, we get back to the two different scaling functions which we discussed in Section 2.4. While we chose the scaling function matching our cone-construction the new construction is based on the tensor-product

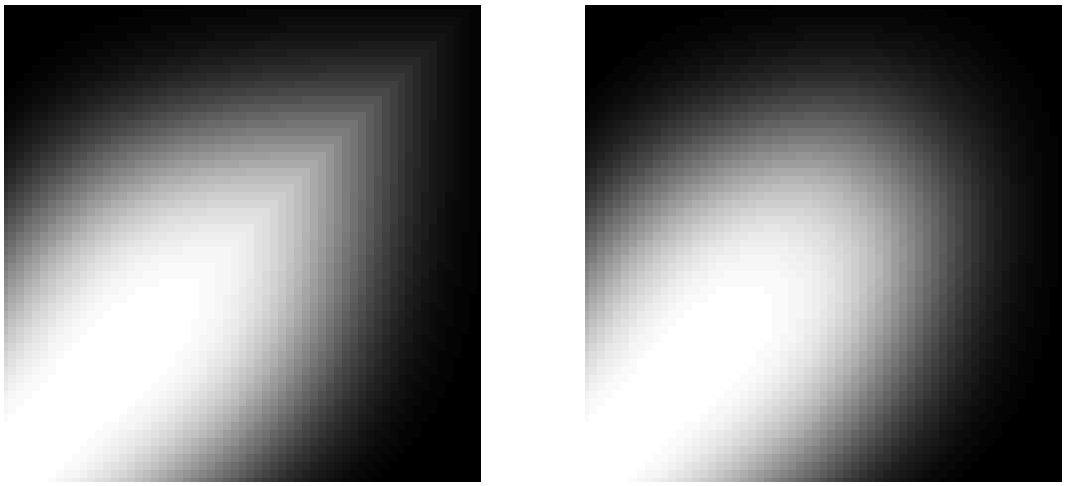

(a) diagonal shearlet in our construction (b) diagonal shearlet in the new construction

Figure 7: Diagonal shearlets in our construction and in the new, smooth construction (Fourier domain)

scaling function $\hat{\Phi}(\omega) = \varphi(\omega_1)\varphi(\omega_2)$. We present the basic steps in the construction of [8] transferred to our setting. In fact, we only need to modify the function ψ_1. We set

$$\hat{\Psi}_1(\omega) := \sqrt{\hat{\Phi}^2(2^{-2}\omega_1, 2^{-2}\omega_2) - \hat{\Phi}^2(\omega_1, \omega_2)}. \tag{24}$$

Clearly, $\hat{\Psi}_1(\omega)$ fulfills $\sum_{j\geq 0} \hat{\Psi}_1^2(2^{-2j}\omega) = 1$ for all $\omega \in \Omega \setminus [-1,1]^2$. We further have that

$$\hat{\Phi}^2(\omega) + \sum_{j\geq 0} \hat{\Psi}_1^2(2^{-2j}\omega) = 1 \quad \text{for } \omega \in \Omega,$$

i.e., this setting provides also a Parseval frame. Fig. 8 shows $\hat{\Psi}_1$. Note that $\hat{\Psi}_1$ is supported in the Cartesian corona $[-4,4]^2 \setminus [-\frac{1}{2},\frac{1}{2}]^2$. The full shearlet Ψ is similar as before:

$$\hat{\Psi}(\omega_1, \omega_2) = \hat{\Psi}_1(\omega_1, \omega_2)\hat{\psi}_2\left(\frac{\omega_2}{\omega_1}\right). \tag{25}$$

The construction of the horizontal, vertical and "diagonal" shearlets is the same as before, besides that the diagonal shearlets are smooth now, see Fig. 7(b).

Before we examine the smoothness of the diagonal shearlets we discuss the differentiability of the remaining shearlets. Due to the construction we only need to analyze the functions $\hat{\psi}_1$ and $\hat{\psi}_2$. We have

$$\hat{\psi}_1(\omega_1) = \sqrt{b^2(2\omega_1) + b^2(\omega_1)} = \begin{cases} 0 & \text{for } |\omega_1| \leq \frac{1}{2} \\ \sin(\frac{\pi}{2} v(2|\omega_1| - 1)) & \text{for } \frac{1}{2} < |\omega_1| < 1 \\ 1 & \text{for } 1 \leq |\omega_1| \leq 2 \\ \cos(\frac{\pi}{2} v(\frac{1}{2}|\omega_1| - 1)) & \text{for } 2 < |\omega_1| < 4 \\ 0 & \text{for } |\omega_1| \geq 4 \end{cases}$$

Figure 8: The new function $\hat{\Psi}_1$ in (24)

and with straight forward differentiation

$$\hat{\psi}_1'(\omega_1) = \begin{cases} 0 & \text{for } |\omega_1| \leq \frac{1}{2} \\ \pi v(2|\omega_1|-1)v'(2|\omega_1|-1)\cos(\frac{\pi}{2}v(2|\omega_1|-1)) & \text{for } \frac{1}{2} < |\omega_1| < 1 \\ 0 & \text{for } 1 \leq |\omega_1| \leq 2 \\ -\frac{\pi}{2}v(\frac{1}{2}|\omega_1|-1)v'(\frac{1}{2}|\omega_1|-1)\sin(\frac{\pi}{2}v(\frac{1}{2}|\omega_1|-1)) & \text{for } 2 < |\omega_1| < 4 \\ 0 & \text{for } |\omega_1| \geq 4. \end{cases}$$

The derivative is continuous if and only if the values at the critical points $\frac{1}{2}, 1, 2, 4$ coincide (for symmetry reasons we can restrict ourselves to the positive range). We have that $v(2 \cdot \frac{1}{2} - 1) = v(0) = 0$ (even $v'(0) = 0$) and $v'(2 \cdot 1 - 1) = v'(1) = 0$ and further $v(\frac{1}{2} \cdot 2 - 1) = v(0) = 0$ and $v'(\frac{1}{2} \cdot 4 - 1) = v'(1) = 0$. Consequently, $\hat{\psi}_1'$ is continuous and in particular $\hat{\psi}_1 \in C^1$. By induction we see that $\hat{\psi}_1^{(n)} \in C^n$ if and only if $v^{(n)}(0) = 0$ and $v^{(n)}(1) = 0$, $n \geq 1$.

For our v in (1) we have $v^{(3)}(1) = 0$ but $v^{(4)}(1) \neq 0$, i.e., $\hat{\psi}_1 \in C^3$.

Similarly, we obtain for $\hat{\psi}_2$ that

$$\frac{\partial \hat{\psi}_2}{\partial \omega_1}(\omega_1, \omega_2) = \begin{cases} -\frac{\omega_2}{\omega_1^2}v'(1+\frac{\omega_2}{\omega_1})\frac{1}{2\sqrt{v(1+\frac{\omega_1}{\omega_2})}} & \text{for } \frac{\omega_2}{\omega_1} \leq 0 \\ \frac{\omega_2}{\omega_1^2}v'(1-\frac{\omega_2}{\omega_1})\frac{1}{2\sqrt{v(1-\frac{\omega_1}{\omega_2})}} & \text{for } \frac{\omega_2}{\omega_1} > 0, \end{cases}$$

where we see that we need $v'(0) = 0$ for the derivative to exist. Thus, the shearlet $\hat{\psi}$ is C^n if $v^{(n)}(0) = v^{(n)}(1) = 0$. This is also valid for the dilated and sheared shearlet $\hat{\psi}^h_{j,k,m}$ (and $\hat{\psi}^v_{j,k,m}$) for $|k| \neq 2^j$. We take a closer look at the diagonal shearlet for $k = -2^j$ where we have

$$\hat{\psi}^{h\times v}_{j,-2^j,m}(\omega) = \begin{cases} \hat{\psi}^h_{j,-2^j,m}(\omega), & \text{for } \omega \in \mathcal{C}^h \\ \hat{\psi}^v_{j,-2^j,m}(\omega), & \text{for } \omega \in \mathcal{C}^v \\ \hat{\psi}^\times_{j,-2^j,m}(\omega), & \text{for } \omega \in \mathcal{C}^\times. \end{cases}$$

Naturally, $\hat{\psi}^{h\times v}_{j,-2^j,m}$ is smooth for $\omega \in \mathcal{C}^h$ and $\omega \in \mathcal{C}^v$. Additionally, $\hat{\psi}^{h\times v}_{j,-2^j,m}(\omega)$ is continuous at the seam lines, but not differentiable there since we have for the partial derivatives of $\hat{\psi}^h_{j,-2^j,m}$ and $\hat{\psi}^v_{j,-2^j,m}(\omega)$ that

$$\begin{aligned}\frac{\partial\hat{\psi}^h_{j,-2^j,m}}{\partial\omega_1}(\omega) &= \hat{\psi}_2(2^j(\frac{\omega_2}{\omega_1}-1))e^{-\frac{2\pi i}{N}(\omega_1 m_1+\omega_2 m_2)}\cdot 2^{-2j}\frac{\partial\hat{\psi}_1}{\partial\omega_1}(2^{-2j}\omega_1)\\ &\quad+\hat{\psi}_1(2^{-2j}\omega_1)e^{-\frac{2\pi i}{N}(\omega_1 m_1+\omega_2 m_2)}(-2^j\frac{\omega_2}{\omega_1^2})\frac{\partial\hat{\psi}_2}{\partial\omega_1}(2^j(\frac{\omega_2}{\omega_1}-1))\\ &\quad+\hat{\psi}_1(2^{-2j}\omega_1)\hat{\psi}_2(2^j(\frac{\omega_2}{\omega_1}-1))(-\frac{2\pi i}{N}m_1)e^{-\frac{2\pi i}{N}(\omega_1 m_1+\omega_2 m_2)}\end{aligned}$$

and

$$\begin{aligned}\frac{\partial\hat{\psi}^v_{j,-2^j,m}}{\partial\omega_1}(\omega) &= \hat{\psi}_1(2^{-2j}\omega_2)\Bigg(e^{-\frac{2\pi i}{N}(\omega_1 m_1+\omega_2 m_2)}(\frac{2^j}{\omega_2})\frac{\partial\hat{\psi}_2}{\partial\omega_1}(2^j(\frac{\omega_1}{\omega_2}-1))\\ &\quad+\hat{\psi}_2(2^j(\frac{\omega_1}{\omega_2}-1))(-\frac{2\pi i}{N}m_1)e^{-\frac{2\pi i}{N}(\omega_1 m_1+\omega_2 m_2)}\Bigg).\end{aligned}$$

For $\omega_1=\omega_2$ we obtain

$$\begin{aligned}\frac{\partial\hat{\psi}^h_{j,-2^j,m}}{\partial\omega_1}(\omega_1,\omega_1) &= e^{-\frac{2\pi i}{N}\omega_1(m_1+m_2)}\cdot\Big(\underbrace{\hat{\psi}_2(0)}_{=1}2^{-2j}\frac{\partial\hat{\psi}_1}{\partial\omega_1}(2^{-2j}\omega_1)\\ &\quad-\hat{\psi}_1(2^{-2j}\omega_1)(\frac{2^j}{\omega_1})\underbrace{\frac{\partial\hat{\psi}_2}{\partial\omega_1}(0)}_{=0}-\hat{\psi}_1(2^{-2j}\omega_1)\underbrace{\hat{\psi}_2(0)}_{=1}(\frac{2\pi i}{N}m_1)\Big)\\ &= e^{-\frac{2\pi i}{N}\omega_1(m_1+m_2)}\cdot\Big(2^{-2j}\frac{\partial\hat{\psi}_1}{\partial\omega_1}(2^{-2j}\omega_1)-(\frac{2\pi i}{N}m_1)\hat{\psi}_1(2^{-2j}\omega_1)\Big)\end{aligned}$$

and

$$\begin{aligned}\frac{\partial\hat{\psi}^v_{j,-2^j,m}}{\partial\omega_1}(\omega_1,\omega_1) &= e^{-\frac{2\pi i}{N}\omega_1(m_1+m_2)}\cdot\Big(\hat{\psi}_1(2^{-2j}\omega_1)(\frac{2^j}{\omega_1})\underbrace{\frac{\partial\hat{\psi}_2}{\partial\omega_1}(0)}_{=0}-\hat{\psi}_1(2^{-2j}\omega_1)\underbrace{\hat{\psi}_2(0)}_{=1}(\frac{2\pi i}{N}m_1)\Big)\\ &= e^{-\frac{2\pi i}{N}\omega_1(m_1+m_2)}\cdot\Big(-(\frac{2\pi i}{N}m_1)\hat{\psi}_1(2^{-2j}\omega_1)\Big).\end{aligned}$$

Obviously, both derivatives do not coincide, thus, our shearlet construction is not smooth for the diagonal shearlets. If we get back to the new construction we obtain for the both partial derivatives

$$\begin{aligned}\frac{\partial\hat{\Psi}^h_{j,-2^j,m}}{\partial\omega_1}(\omega) &= 2^{-2j}\frac{\partial\hat{\Psi}_1}{\partial\omega_1}(2^{-2j}\omega)\hat{\psi}_2(2^j(\frac{\omega_2}{\omega_1}-1))e^{-\frac{2\pi i}{N}(\omega_1 m_1+\omega_2 m_2)}\\ &\quad-2^j\frac{\omega_2}{\omega_1^2}\hat{\Psi}_1(2^{-2j}\omega)\frac{\partial\hat{\psi}_2}{\partial\omega_1}(2^j(\frac{\omega_2}{\omega_1}-1))e^{-\frac{2\pi i}{N}(\omega_1 m_1+\omega_2 m_2)}\\ &\quad-\frac{2\pi i}{N}m_1\hat{\Psi}_1(2^{-2j}\omega)\hat{\psi}_2(2^j(\frac{\omega_2}{\omega_1}-1))e^{-\frac{2\pi i}{N}(\omega_1 m_1+\omega_2 m_2)}\end{aligned}$$

and

$$\begin{aligned}\frac{\partial \hat{\Psi}^v_{j,-2^j,m}}{\partial \omega_1}(\omega) &= 2^{-2j}\frac{\partial \hat{\Psi}_1}{\partial \omega_1}(2^{-2j}\omega)\hat{\psi}_2(2^j(\frac{\omega_1}{\omega_2}-1))e^{-\frac{2\pi i}{N}(\omega_1 m_1+\omega_2 m_2)}\\ &+ (\frac{2^j}{\omega_2})\hat{\Psi}_1(2^{-2j}\omega)\frac{\partial \hat{\psi}_2}{\partial \omega_1}(2^j(\frac{\omega_1}{\omega_2}-1))e^{-\frac{2\pi i}{N}(\omega_1 m_1+\omega_2 m_2)}\\ &- \frac{2\pi i}{N}m_1\hat{\Psi}_1(2^{-2j}\omega)\hat{\psi}_2(2^j(\frac{\omega_1}{\omega_2}-1))e^{-\frac{2\pi i}{N}(\omega_1 m_1+\omega_2 m_2)}.\end{aligned}$$

With $\omega_1 = \omega_2$ we obtain further

$$\begin{aligned}\frac{\partial \hat{\Psi}^h_{j,-2^j,m}}{\partial \omega_1}(\omega_1,\omega_1) &= 2^{-2j}\frac{\partial \hat{\Psi}_1}{\partial \omega_1}(2^{-2j}\omega_1,2^{-2j}\omega_1)\underbrace{\hat{\psi}_2(0)}_{=1}e^{-\frac{2\pi i}{N}\omega_1(m_1+m_2)}\\ &- 2^j\frac{\omega_2}{\omega_1^2}\hat{\Psi}_1(2^{-2j}\omega_1,2^{-2j}\omega_1)\underbrace{\frac{\partial \hat{\psi}_2}{\partial \omega_1}(0)}_{=0}e^{-\frac{2\pi i}{N}\omega_1(m_1+m_2)}\\ &- \frac{2\pi i}{N}m_1\hat{\Psi}_1(2^{-2j}\omega_1,2^{-2j}\omega_1)\underbrace{\hat{\psi}_2(0)}_{=1}e^{-\frac{2\pi i}{N}\omega_1(m_1+m_2)}\end{aligned}$$

and

$$\begin{aligned}\frac{\partial \hat{\Psi}^v_{j,-2^j,m}}{\partial \omega_1}(\omega_1,\omega_1) &= 2^{-2j}\frac{\partial \hat{\Psi}_1}{\partial \omega_1}(2^{-2j}\omega_1,2^{-2j}\omega_1)\underbrace{\hat{\psi}_2(0)}_{=1}e^{-\frac{2\pi i}{N}\omega_1(m_1+m_2)}\\ &+ (\frac{2^j}{\omega_2})\hat{\Psi}_1(2^{-2j}\omega_1,2^{-2j}\omega_1)\underbrace{\frac{\partial \hat{\psi}_2}{\partial \omega_1}(0)}_{=0}e^{-\frac{2\pi i}{N}\omega_1(m_1+m_2)}\\ &- \frac{2\pi i}{N}m_1\hat{\Psi}_1(2^{-2j}\omega_1,2^{-2j}\omega_1)\underbrace{\hat{\psi}_2(0)}_{=1}e^{-\frac{2\pi i}{N}\omega_1(m_1+m_2)}.\end{aligned}$$

It can be easily seen that both derivatives coincide if and only if $\frac{\partial \hat{\psi}_2}{\partial \omega_1}(0) = 0$ since then the second term vanishes. The same result is obtained for partial derivative with respect to ω_2. Consequently, the new construction is smooth everywhere.

Remark 3.2. *As we have seen the smoothness of the shearlets depends strongly on the smoothness of the function v. The v we have used was constructed to provide shearlets in C^3. The first three derivatives at 0 and 1 should be equal to zero, i.e., $v'(x) = c \cdot x^3(x-1)^3$. With $v(1) = 1$ and straight forward integration one obtain $c = -140$ and the function v as in (1).*

Higher grades of smoothness can easily be obtained by creating a new v by setting $v'(x) = c \cdot x^k(x-1)^k$. These shearlets would be in C^k.

Note that due to our discretization $t = m$ we have a unique handling of both the horizontal and the vertical cone and do not have to make any adjustments for the diagonal shearlets, in contrast to the discretization $t = A_{a_j}S_{s_{jk}}m$ where you have different discretizations for t in

the horizontal and in the vertical cone. Consequently, some adjustments have to be made for the diagonal shearlets.

Smooth shearlets are well-located in time. To show the difference we present in Fig. 9(a) the "old" shearlet in the time domain and in comparison in Fig. 9(b) the new construction in the time domain. The non-smooth construction is slightly worse located. The shearlet coefficients

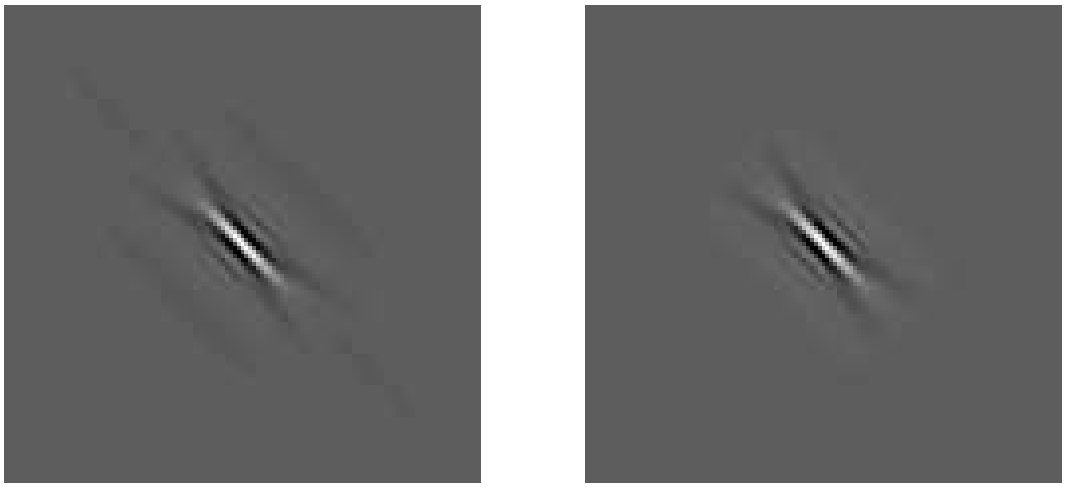

(a) diagonal shearlet in our construction, time domain

(b) diagonal shearlet in the new construction, time domain

Figure 9: diagonal shearlets in our construction and in the new, smooth construction (Time domain)

of, e.g., a diagonal line only show marginal differences such that for practical applications it is irrelevant which construction is used.

3.5 Implementation details

The implementation of the shearlet transform follows very closely the details described here. As we see in (22) and (23) for both directions of the transform the spectra of ψ and ϕ are needed for all scales j and all shears s on "all" sets. We precompute these spectra to use them for both directions.

Up to now our implementation only supports quadratic images, i.e., $M = N$ (see Remark 3.4 for a short discussion on this topic).

3.5.1 Indexing

To reduce the number of parameters we introduce one index i which replaces the parameters κ, j and k. We set $i = 1$ for the low-pass part. We continue with the lowest frequency band, i.e., $j = 0$. The different "cones" and shear parameters represent the different "directions" of the shearlet. For illustration we reduce the shearlet to a line which is rotated counter-clockwise around the center and assign the index i accordingly. In each frequency band we start in the

horizontal position, i.e., $\kappa = h$ and $k = 0$, and increase i by one. For each $k = -1, \dots, -2^j + 1$ we continue increasing the index by one. The line is now almost in a 45° angle (or a line with slope 1). The next index is assigned to the combined shearlet "$h \times v$" at the seam line which covers the "diagonal" for $k = -2^j$. We continue in the vertical cone for $k = -2^j + 1, \dots, 2^j - 1$. Next is again the combined shearlet for $k = 2^j$. With decreasing shear, i.e., $k = 2^j, \dots, 1$, we finish the indexing for this frequency-band and continue with the next one.

Summarizing we have always one index for the low-pass part. In each frequency band we have 2 indices (or shearlets) for the diagonals ($k = \pm 2^j$). In each cone we have $1 + 2 \cdot (2^j - 1) = 2^{j+1} - 1$ shearlets. For the scale j we have $2 \cdot (2^{j+1} - 1) + 2 = 2^{j+2}$ shearlets. The following table lists the number of shearlets for each j.

low-pass	$j = 0$	$j = 1$	$j = 2$	$\cdots$
1	4	8	16	$\cdots$

With a maximum scale $j_0 - 1$ the number of all indices η is

$$\eta = 1 + \sum_{j=0}^{j_0-1} 2^{j+2} = 1 + 4 \sum_{j=0}^{j_0-1} 2^j = 1 + 4 \cdot (2^{j_0} - 1) = 2^{j_0+2} - 3. \tag{26}$$

For each index the spectrum is computed on a grid of size $N \times N$. We store all indices in a three-dimensional matrix of size $N \times N \times \eta$. The first both components refer to the ω_2 and ω_1 coordinates and the third component is the respective index. Consequently, an image f of size $N \times N$ is oversampled to an image of size $N \times N \times \eta$. In particular we have an oversampling factor of η. The following table lists η for $j_0 = 1, \dots, 4$.

j_0	1	2	3	4	$\cdots$
η	5	13	29	61	$\cdots$

Note that j_0 is the *number* of scales, the highest scale parameter j is always $j_0 - 1$, i.e., we have the scale parameters $0, \dots, j_0 - 1$. The function `helper/shearletScaleShear` provides various possibilities to compute the index i from a and s or from j and k and vice versa. See documentation inside the file for more information.

3.5.2 Computation of spectra

We compute the spectra $\hat{\psi}_{j,k,m}$ as discrete versions of the continuous functions, i.e., we compute the values on a finite discrete lattice Ξ of size $N \times N$. With the functions defined as in (4) and (6) we may not take $\Xi = \Omega$ as this would destroy the frame property. The question is how to choose X (such that $\Xi \in [-X, X)^{N \times N}$) or the distance Δ between to grid points, respectively.

The use of Theorem 2.2 in the proof of Theorem 3.1 was not completely correct. We have that $\operatorname{supp} \hat{\psi}_1(\omega) = [\frac{1}{2}, 4] = [2^{-1}, 2^2]$ and $\hat{\psi}_1 = 1$ for $\omega \in [1, 2] = [2^0, 2^1]$. For the scaled

version we further have $\operatorname{supp}\hat{\psi}_1(2^{-2j}\omega) = [2^{2j-1}, 2^{2j+2}]$ and $\hat{\psi}_1(2^{-2j}\omega) = 1$ for $\omega \in [2^{2j}, 2^{2j+1}]$. Consequently, we can conclude

$$\sum_{j=0}^{j_0-1} |\hat{\psi}_1(2^{-2j}\omega)|^2 = \begin{cases} 0 & \text{for } |\omega| \leq \frac{1}{2} \\ \sin^2\left(\frac{\pi}{2} v(2\omega - 1)\right) & \text{for } \frac{1}{2} < |\omega| < 1 \\ 1 & \text{for } 1 \leq |\omega| \leq 2^{2(j_0-1)+1} \\ \cos^2\left(\frac{\pi}{2} v(2^{-2j_0-1}\omega - 1)\right) & \text{for } 2^{2(j_0-1)+1} < |\omega| < 2^{2(j_0-1)+2} \\ 0 & \text{for } |\omega| \geq 2^{2(j_0-1)+2}. \end{cases}$$

We see that the sum is equal to 1 for a wide range of ω. As we have seen the part for $|\omega| < 1$ where the sum increases from 0 to 1 matches with the decreasing part of the scaling function (see (15)). But we also have a decay for $|\omega| > 2^{2(j_0-1)+1}$ where there is no compensation to 1 since there are no higher scales. Keeping this decay would violate the frame property.

Consequently, X must be less or equal than $2^{2(j_0-1)+1} = 2^{2j_0-1}$ which implies the decay to be "outside" the image. We set $X = 2^{2j_0-1}$. Additionally, if we get back to the lowest scale it is reasonable to set $\Delta \leq 1$ since otherwise there would be to less grid points in $\operatorname{supp}\hat{\psi}_1$.

To compute the grid and the spectra we assume that $N = 2n + 1$ is odd. We then have a symmetric grid around 0, hence, we have n grid points in the negative range and n grid points in the positive range and one grid point at 0. If N is given even we increase it by 1. After computing grid and spectra we neglect the last row and column to retain the original image size. Having $n = \frac{N-1}{2}$ grid points for the positive range and the maximal distance between two grid points $\Delta = 1$ we get

$$X = 2^{2j_0-1} = \frac{N-1}{2} \Longrightarrow j_0 = \frac{1}{2}\log_2(N-1).$$

Since j_0 is the (scalar!) number of scales, we set for the number of scales (as used above) $j_0 := \lfloor \frac{1}{2}\log_2(N) \rfloor$. In the following table we list the number of scales for all image sizes $N = 4 \ldots, 1024$

N	$4, \ldots, 15$	$16, \ldots, 63$	$64, \ldots, 255$	$256, \ldots, 1023$	1024
j_0	1	2	3	4	5

.

With j_0 fixed we can compute the second parameter Δ. As we have seen the highest value in the grid should be $X = 2^{2j_0-1}$. For an odd N the grid ranges from $[-X, X]$ and for an even grid we have the range $[-X, X) = [-X, X - \Delta]$. We assume again an odd N, thus, the interval $[-X, X]$ should be divided in N grid points including the bounds $-X$ and X what leads to $N - 1$ subintervals and

$$\Delta = \frac{2 \cdot X}{N-1} = \frac{2 \cdot 2^{2j_0-1}}{N-1} = \frac{2^{2j_0}}{N-1}.$$

Where $\Delta = 1$ if $N = 2^{2j_0} + 1$ and $\Delta > \frac{1}{4}$, i.e., $\frac{1}{4} < \Delta \leq 1$. Thus, for the same number of scales we obtain a better resolution with increasing image size.

It seems a little awkward to discretize $\hat{f}$ and $\hat{\psi}$ on different lattices. However, with this auxiliary construction the definition and properties of the shearlet $\hat{\psi}$ is much more convenient. Additionally the shearlets are now independent of the parameter Δ (or other grid properties). Anyway, to circumvent the imperfection with two lattices we can now formerly also discretize $\hat{\psi}(\Delta\omega)$ on Ω instead of $\hat{\psi}(\omega)$ on Ξ and obtain the same spectra.

Remark 3.3. *The spectra depend strongly on the image size. In particular, if we reduce the image size a bit but still have the same number of scales the resolution of the different frequency bands varies. This may be not wanted for comparison issues. To circumvent this one could chose the grid according to the highest image size (for the respective number of scales) and drop the boundaries for smaller images. This would however lead to a very small high frequency band for smaller images. In our current implementation this frequency band is as large as possible.*

Remark 3.4. *The theoretical results shown are valid for both square images and rectangular images, i.e., we have $\mathcal{I}$ and Ω of size $M \times N$. However, our implementation only supports square images. For the extension to rectangular images some questions remain. The first question is what the "diagonal" in a discrete rectangular setting is, i.e., the "diagonal" shearlets have to be handled carefully. More tricky is the question how to handle the different sizes in the both directions with respect to the size of the grid especially if $M \ll N$ (or $M \gg N$) and the number of scales. Possible are an equispaced grid in both directions and thus less scales in one direction or the same number of scales but a non-equispaced grid what would lead to rectangular frequency bands. Depending on the application both seems useful. We hope to implement rectangular shearlets in a future version of the software.*

3.6 Short documentation

Every file contained in the package is commented, see there for details on the arguments and return values. Thus, we only want to comment on the two important functions.

The transform for an image `A`$\in \mathbb{C}^{N \times N}$ is called with the following command

```
[ST,Psi] = shearletTransformSpect(A,numOfScales,shearlet_spect
   ,shearlet_arg)
```

where `numOfscales`, `shearlet_spect` and `shearlet_arg` are optional arguments. If only `A` is given the number of scales j_0 is computed from the size of `A`, i.e., $j_0 = \lfloor \frac{1}{2} \log_2(N) \rfloor$ and the shearlet with (4) and (6) is used. On the other hand `numOfScales` can be used two-fold. If given as a scalar value it simply states the number of scales to consider. On the other hand we can provide precomputed shearlet spectra which are then used for the computation of the transform. Observe that the shearlet spectra only depend on the size of the image and the number of scales, thus, they are cached and reused if the function is called with an image of same size again. The variable `ST` contains the shearlet coefficients as a three-dimensional matrix of size $N \times N \times \eta$ with the third dimension ordered as described in section 3.5.1. `Psi` is of same size and contains the respective shearlet spectra $\hat{\psi}^{\kappa}_{j,k,0}$.

With the parameters `shearlet_spect` and `shearlet_arg` other shearlets can be used to compute the spectra. Included in the software is the '`meyerShearletSpect`' as default shearlet (based on (4) and (6)) and '`meyerNewShearletSpect`' for the new smooth construction (see (25)). The parameter `shearlet_arg` is not used in both cases.

The application of other shearlet spectra is very straight forward. One the one hand one can simply compute them externally in the matrix `Psi` and provide them as the parameter `numOfScales`. On the other hand it is possible to provide an own function '`myShearletSpect`' (with arbitrary name) with the function head

```
Psi = myShearletSpect(x,y,a,s,shearlet_arg)
```

that computes the spectrum `Psi` for given (meshgrids) `x` and `y` for scalar scale `a` and shear `s` and (optional) parameter `shearlet_arg`. For `shearlet_arg='scaling'` it should return the scaling function. To obtain a reasonable transform the shearlet should provide a Parseval frame. To check this just compute (and plot) `sum(abs(Psi).^2,3)-1`. The values should be close to zero (see Fig. 11(a)). Call the shearlet transform with the new shearlet spectrum by setting the variable `sherlet_spect` to `myShearletSpect` or whatever you chose as the name of your shearlet function.

The inverse transform is called with the command

```
A = inverseShearletTransformSpect(ST,Psi,shearlet_spect,
    shearlet_arg)
```

for the shearlet coefficients `ST`. As the second argument the shearlet spectra `Psi` should be provided for faster computations, if not given, the spectra are computed with default values or given spectrum `shearlet_spect`.

3.7 Download & Installation

The MATLAB-Version of the toolbox is available for free download at

`http://www.mathematik.uni-kl.de/~haeuser/FFST`

The zip-file contains all relevant files and folders. Simply unzip the archive and add the folder (with subfolders!) to your MATLAB-path.

The folder **FFST** contains the main files for the both directions of the transform. The included shearlets are stored in the folder **shearlets**. The folder **helper** contains some helper functions. To create simple geometric structures some functions are provided in **create**. See `contents.m` and the comments in each file for more information.

The following listing shows the subdirectories and the respective files

```
FFST/
├── create/
│   ├── myBall.m
│   ├── myPicture.m
│   ├── myPicture2.m
│   ├── myRhombus.m
│   └── mySquare.m
├── helper/
│   ├── coneIndicator.m
│   ├── scalesShearsAndSpectra.m
│   └── shearletScaleShear.m
└── shearlets/
    └── bump.m
```

```
    ├── meyeraux.m
    ├── meyerNewShearletSpect.m
    ├── meyerScaling.m
    ├── meyerScalingSpect.m
    ├── meyerShearletSpect.m
    └── meyerWavelet.m
├── inverseShearletTransformSpect.m
└── shearletTransformSpect.m
```

If everything is installed correctly run `simple_example` for testing. The result should look like Fig. 10.

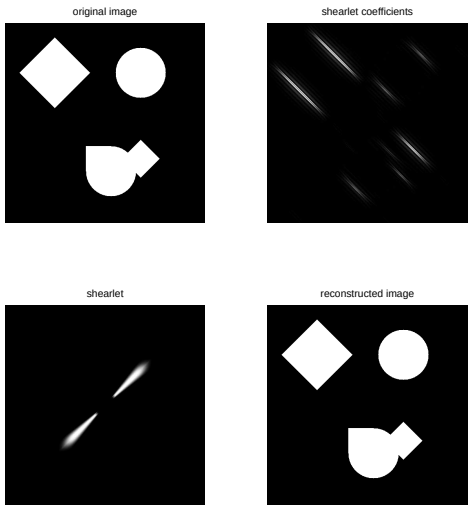

Figure 10: Result of script `simple_example`.

3.8 Performance

To evaluate the performance and the exactness of our implementation we present the following figures. In Fig. 11(a) we investigate the numerical tightness of the frame. The figure shows the difference between the square sum of the shearlets and 1, i.e.,

$$\sum_{\kappa\in\{h,v\}}\sum_{j=0}^{j_0-1}\sum_{k=-2^j}^{2^j}|\hat{\psi}^{\kappa}_{j,k,0}|^2+\sum_{j=0}^{j_0-1}\sum_{k=\pm 2^j}|\hat{\psi}^{h\times v}_{j,k,0}|^2+|\hat{\phi}_0|^2-1$$

The biggest deviation is about $8\cdot 10^{-15}$ which is 40 times the machine precision. The second figure Fig. 11(b) shows the difference between the original image and the back transformed image of a random image, i.e., the exactness of the forward and backwards transform. Here the biggest difference is about $2\cdot 10^{-15}$ or approximately 10 times the machine precision. Surprisingly this is even better than the tightness of the used frame.
Next we want to compare the speed of our implementation for different image sizes $N\times N$ for $N=2^i$ with $i=5,\dots,10$. In the first run all the spectra are computed, thus, this run

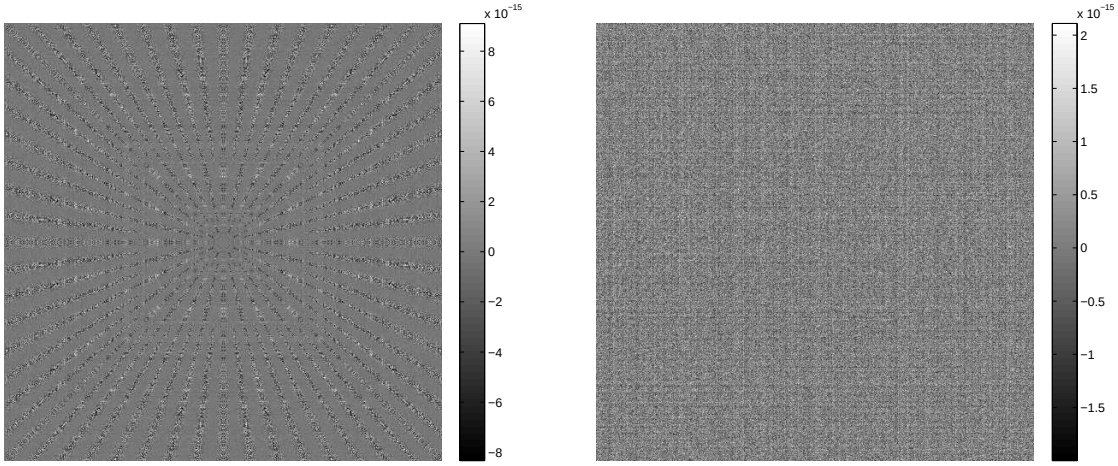

(a) frame tightness

(b) transform exactness

Figure 11: Comparison of frame tightness and the exactness of the transform

takes significantly longer than the second and all following runs. The different run times are shown in Fig. 12 with logarithmic scale. To get reasonable results we take the average time over 5 "first" runs (with deleting the cache, solid line) and 5 "second runs" (dashed line). The dotted line shows the time needed for the inverse shearlet transform. Since no spectra have to be computed here the time is approximately the same as for the second runs of the transform self. We compare the runtimes with *ShearLab*[2], the only so far publicly available shearlet implementation. The dash-dotted line in Fig. 12 shows that ShearLab is slightly slower then our implementation (in the first run). Observe that no time could be measured for $N = 1024$ with ShearLab. In our implementation it is possible to compute the shearlet transform for arbitrary image sizes, whereas in ShearLab the transform is only possible for given image sizes. All tests were performed on an Intel i7 870 (Quad Core, each 2.93 GHz) with 8 GB RAM on Ubuntu 10.04 with MATLAB R2011b (64-bit).

3.9 Remarks

1. In [16] and the respective implementation *ShearLab* a pseudo-polar Fourier transform is used to implement a discrete (or digital) shearlet transform. For the scale a and the shear s the same discretization is used. But for the translation t the authors set $t_{j,k,m} := A_{a_j} S_{s_{j,k}} m$ where we in contrast simply set $t_m := m$ (see (17)). Thus, their discrete shearlet becomes

$$\hat{\tilde{\psi}}_{j,k,m}(\omega) = \hat{\psi}(A_{a_j} S^{\mathrm{T}}_{s_{j,k}} \omega) e^{-2\pi i \langle \omega, A_{a_j} S_{s_{j,k}} m \rangle} = \hat{\psi}(A_{a_j} S^{\mathrm{T}}_{s_{j,k}} \omega) e^{-2\pi i \langle S^{\mathrm{T}}_{s_{j,k}} A_{a_j} \omega, m \rangle}.$$

   Since the operation $S^{\mathrm{T}}_{s_{j,k}} A_{a_j} \omega$ would destroy the pseudo-polar grid a "slight" adjustment is made and the exponential term is replaced by

$$e^{-2\pi i \langle (\theta \circ S^{-\mathrm{T}}_{s_{j,k}}) S^{\mathrm{T}}_{s_{j,k}} A_{a_j} \omega, m \rangle}$$

[2] http://www.shearlab.org

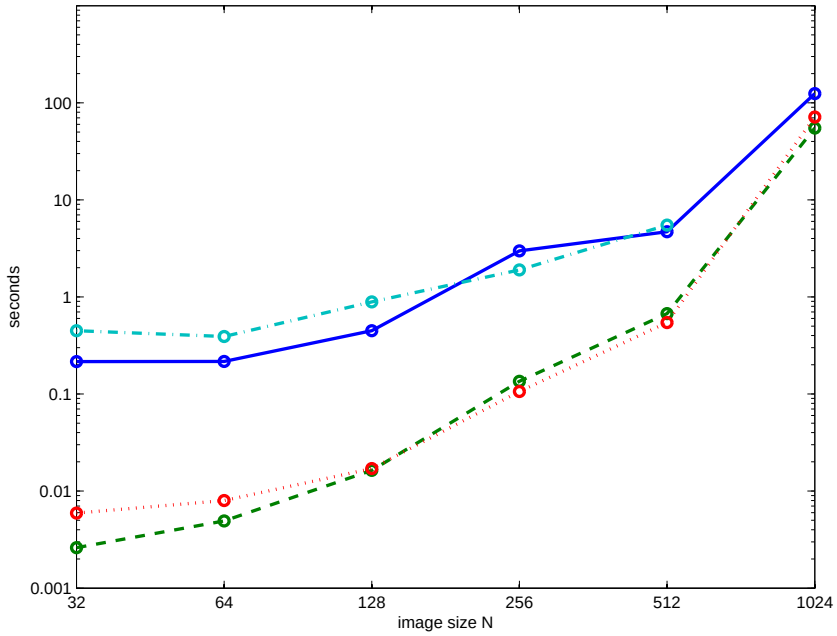

Figure 12: run times for different image sizes, "first run" (solid), "second" run (dashed), inverse (dotted), ShearLab (dashed-dotted, no time for $N = 1024$).

with $\theta\colon \mathbb{R} \setminus \{0\} \times \mathbb{R} \to \mathbb{R} \times \mathbb{R}$ and $\theta(x, y) = (x, \frac{y}{x})$ such that

$$e^{-2\pi i \langle (\theta \circ S_{s_{j,k}}^{-\mathrm{T}}) S_{s_{j,k}}^{\mathrm{T}} A_{a_j} \omega, m \rangle} = e^{-2\pi i \left\langle \left(a_j \omega_1, \sqrt{a_j} \frac{\omega_2}{\omega_1} \right), m \right\rangle}.$$

With this adjustment the last step of the shearlet transform can be obtained with a standard inverse fast Fourier transform (similar as in our implementation). Unfortunately this is no longer related to translations of the shearlets in the time domain.

2. We are aware of our larger oversampling factor in comparison with, e.g., *ShearLab*. Having 4 scales we obtain 61 images of the same size as the original image. But since shearlets are designed to detect edges in images we like to avoid any down-sampling and keep translation invariance. A possibility to reduce the memory usage would be to use the compact support of the shearlets in the frequency domain and only compute them on a "relevant" region. But we then would also have to store the position and size of each region what decreases the memory savings and would make the implementation a lot more complicated.

Acknowledgement

The author thanks Tomas Sauer (University of Gießen) for his support at the beginning of this project.

References

[1] E. Candes, L. Demanet, D. Donoho, and L. Ying. Fast discrete curvelet transforms. *Multiscale Modeling Simulation*, 5(3), 2006.

[2] E. J. Candes and D. L. Donoho. Ridgelets: a key to higher-dimensional intermittency? *Philosophical Transactions of the London Royal Society*, 357:2495–2509, 1999.

[3] O. Christensen. *An Introduction to Frames and Riesz Bases*. Birkhauser, 2003.

[4] S. Dahlke, G. Kutyniok, P. Maass, C. Sagiv, H.-G. Stark, and G. Teschke. The uncertainty principle associated with the continuous shearlet transform. *International Journal on Wavelets Multiresolution and Information Processing*, 6:157–181, 2008.

[5] S. Dahlke, G. Kutyniok, G. Steidl, and G. Teschke. Shearlet coorbit spaces and associated banach frames. *Applied and Computational Harmonic Analysis*, 27(2):195–214, 2009.

[6] K. Guo, G. Kutyniok, and D. Labate. Sparse multidimensional representations using anisotropic dilation und shear operators. *Wavelets und Splines (Athens, GA, 2005), G. Chen und M. J. Lai, eds., Nashboro Press, Nashville, TN*, pages 189–201, 2006.

[7] K. Guo and D. Labate. Characterization and analysis of edges using the continuous shearlet transform. *SIAM Journal on Imaging Sciences*, 2(3):959–986, 2009.

[8] K. Guo and D. Labate. The construction of smooth parseval frames of shearlets. 2011.

[9] S. Häuser and G. Steidl. Convex multilabel segmentation with shearlet regularization. *Preprint University of Kaiserslautern*, 2011.

[10] G. Kutyniok, K. Guo, and D. Labate. Sparse multidimensional representations using anisotropic dilation and shear operators. *Wavelets und Splines (Athens, GA, 2005), G. Chen und MJ Lai, eds., Nashboro Press, Nashville, TN*, pages 189–201, 2006.

[11] G. Kutyniok and W. Lim. Image separation using wavelets and shearlets. *Curves and Surfaces (Avignon, France, 2010), Lecture Notes in Computer Science*, to appear.

[12] D. Labate, G. Easley, and W. Lim. Sparse directional image representations using the discrete shearlet transform. *Applied and Computational Harmonic Analysis*, 25(1):25–46, 2008.

[13] W. Lim, G. Kutyniok, and X. Zhuang. Digital shearlet transforms. *Shearlets: Multiscale Analysis for Multivariate Data*, to appear.

[14] S. Mallat. *A Wavelet Tour of Signal Processing: The Sparse Way*. Academic Press, 2008.

[15] Y. Meyer. *Oscillating Patterns in Image Processing and Nonlinear Evolution Equations*, volume 22. AMS, Providence, 2001.

[16] M. Shahram, G. Kutyniok, and X. Zhuang. Shearlab: A rational design of a digital parabolic scaling algorithm. submitted.

[17] S. Yi, D. Labate, G. Easley, and H. Krim. A shearlet approach to edge analysis and detection. *Image Processing, IEEE Transactions on*, 18(5):929–941, 2009.